Dissipative hidden sector dark matter

R. Foot[*] and S. Vagnozzi[†]

*ARC Centre of Excellence for Particle Physics at the Terascale, School of Physics,
University of Melbourne, Victoria 3010, Australia*

A simple way of explaining dark matter without modifying known Standard Model physics is to require the existence of a hidden (dark) sector, which interacts with the visible one predominantly via gravity. We consider a hidden sector containing two stable particles charged under an unbroken $U(1)'$ gauge symmetry, hence featuring dissipative interactions. The massless gauge field associated with this symmetry, the dark photon, can interact via kinetic mixing with the ordinary photon. In fact, such an interaction of strength $\epsilon \sim 10^{-9}$ appears to be necessary in order to explain galactic structure. We calculate the effect of this new physics on big bang nucleosynthesis and its contribution to the relativistic energy density at hydrogen recombination. We then examine the process of dark recombination, during which neutral dark states are formed, which is important for large-scale structure formation. Galactic structure is considered next, focusing on spiral and irregular galaxies. For these galaxies we modeled the dark matter halo (at the current epoch) as a dissipative plasma of dark matter particles, where the energy lost due to dissipation is compensated by the energy produced from ordinary supernovae (the core-collapse energy is transferred to the hidden sector via kinetic mixing induced processes in the supernova core). We find that such a dynamical halo model can reproduce several observed features of disk galaxies, including the cored density profile and the Tully-Fisher relation. We also discuss how elliptical and dwarf spheroidal galaxies could fit into this picture. Finally, these analyses are combined to set bounds on the parameter space of our model, which can serve as a guideline for future experimental searches.

I. INTRODUCTION

A variety of observations suggest the existence of non-baryonic dark matter in the Universe. Among these are measurements of the rotation curves of spiral galaxies, which are asymptotically flat [1]. Dark matter is also required to explain the cosmic microwave background (CMB) anisotropy spectrum (particularly the structure of the acoustic peaks), the matter power spectrum and large-scale structure (LSS) formation (see e.g. [2]). Cosmological observations can be explained within the framework of the Friedmann-Robertson-Walker (FRW) model (see e.g. [3]), which assumes isotropy and homogeneity of the Universe on large scales. Comparisons with observations require the total dark matter mass to be approximately 5 times that of baryonic matter.

The particle physics underlying dark matter is unknown but a promising possibility, widely discussed in recent literature (see e.g. [4–7]) is that dark matter resides in a hidden sector. That is, an additional sector containing particles and forces, which interact with the known Standard Model particle content predominantly via gravity. A special case is mirror dark matter (MDM), where the hidden sector is exactly isomorphic to the Standard Model

[8]. It has been shown that MDM can, under suitable assumptions and initial conditions, reproduce the successes of collisionless cold dark matter (CDM) on large scales, while deviating on small scales. This is important because such a model has the potential to address apparent short-comings of collisionless CDM such as inferred cores in dark matter halos and the missing satellites problem [9,10].

Mirror dark matter is self-interacting due to an unbroken $U(1)'$ interaction (mirror electromagnetism). The associated gauge boson, the mirror photon, is massless, which implies that MDM is dissipative. Dissipative dark matter is a possible scenario, provided that there exists a substantial heat source that can replace the energy lost due to dissipative interactions. It has been argued [11] that ordinary supernovae can provide such a heat source provided photon-mirror photon kinetic mixing exists. More in-depth studies of this possibility [12] have shown that the model can reproduce several observational properties of disk galaxies. MDM also seems to be capable of explaining the positive results from the direct detection experiments, especially the annual modulation signals observed by DAMA [13] and CoGeNT [14], consistently with results from the other experiments [15,16]. For an up-to-date review and a more detailed bibliography see [17].

It is possible that dark matter might arise from a more generic hidden sector with qualitatively similar features.

[*]rfoot@unimelb.edu.au
[†]svagnozzi@physics.unimelb.edu.au, vagnozzi@nbi.dk

As long as the hidden sector contains an unbroken $U(1)'$ gauge interaction, dissipative dark matter can arise. The simplest such generic hidden sector model contains two massive states, interacting with the $U(1)'$ gauge field (the *dark photon*), with *a priori* unknown $U(1)'$ charges and masses. Such a model can then closely resemble MDM, with the lighter state corresponding to the mirror electron and the heavier state corresponding to mirror nuclei. Kinetic mixing can couple the massless $U(1)'$ gauge field with the ordinary photon. The fundamental physics is described by five free parameters. Our aim is to constrain this five-dimensional parameter space using early universe cosmology and galactic structure considerations.

The outline of this article, then, is as follows. In Sec. II we define the model and examine some of its properties. Sections III and IV are devoted to studying its early universe phenomenology, focusing in particular on how big bang nucleosynthesis (BBN) and the onset of structure formation are affected. Section V is dedicated to analyzing the model in the context of galactic structure. Finally, in Sec. VI we draw on the analyses of the previous sections to summarize the constraints on the model, and in Sec. VII we give some concluding remarks.

II. TWO-COMPONENT HIDDEN SECTOR DARK MATTER

The model considered incorporates a hidden sector featuring an unbroken $U(1)'$ gauge interaction. This means there is a massless gauge boson, called the *dark photon* (γ_D). The hidden sector will also contain two stable dark matter particles, F_1 and F_2, taken to be Dirac fermions, with masses m_{F_1} and m_{F_2}. These two particles are assumed to be charged under the $U(1)'$ gauge group, with charges Q'_{F_1} and Q'_{F_2}, opposite in sign but not necessarily equal in magnitude.

In the early universe, the $U(1)'$ interactions would be expected to efficiently annihilate the symmetric component, meaning that the abundance of F_1 and F_2 dark matter is set by its particle-antiparticle asymmetry. This is an example of *asymmetric* dark matter, which has been extensively discussed in recent literature [18]. Dark matter asymmetry and local neutrality of the Universe then imply

$$n_{F_1} Q'_{F_1} + n_{F_2} Q'_{F_2} = 0, \qquad (1)$$

where n_{F_1} and n_{F_2} are the number densities of F_1 and F_2, respectively. This is, of course, quite analogous to the situation with ordinary matter ($F_1 \sim$ electron, $F_2 \sim$ proton).

The only possible renormalizable and gauge-invariant interaction coupling the ordinary particles with the dark sector is the $U(1)' - U(1)_Y$ kinetic mixing term [19]. Including this term, the full Lagrangian of our model is[1]

---

[1]Here and throughout the article, natural units with $\hbar = c = k_B = 1$ will be used.

$$\mathcal{L} = \mathcal{L}_{\text{SM}} - \frac{1}{4} F'^{\mu\nu} F'_{\mu\nu} + \bar{F}_1 (iD_\mu \gamma^\mu - m_{F_1}) F_1$$
$$+ \bar{F}_2 (iD_\mu \gamma^\mu - m_{F_2}) F_2 - \frac{\epsilon'}{2} F^{\mu\nu} F'_{\mu\nu}, \qquad (2)$$

where $\mathcal{L}_{\text{SM}}$ denotes the $SU(3)_c \otimes SU(2)_L \otimes U(1)_Y$ gauge invariant Standard Model Lagrangian which describes the interactions of the ordinary particles. Also, $F'_{\mu\nu} = \partial_\mu A'_\nu - \partial_\nu A'_\mu$ [$F_{\mu\nu} = \partial_\mu B_\nu - \partial_\nu B_\mu$] is the field-strength tensor associated with the $U(1)'$ [$U(1)_Y$] gauge interaction, A'_μ [$B_\mu = \cos\theta_w A_\mu + \sin\theta_w Z_\mu$] being the relevant gauge field. The two dark fermions are described by the quantum fields F_j and $D_\mu F_j = \partial_\mu F_j + ig' Q'_j A'_\mu F_j$, where g' is the coupling constant relevant to this gauge interaction ($j = 1, 2$). The dark fermions are stable which is a consequence of the $U(1)'$ gauge symmetry and an accidental $U(1)$ global symmetry (implying conservation of F_1 and F_2 numbers). This is reminiscent of how $U(1)_Q$ and the accidental baryon number symmetries arise in the Standard Model and how they stabilize the electron and proton. This is quite a general feature of hidden sector dark matter models and illustrates why they are so appealing theoretically: they typically predict a spectrum of massive, dark and stable particles.

The interactions of F_1 with the dark photon are characterized by the dark fine structure constant: $\alpha' \equiv (g' Q'_{F_1})^2 / 4\pi$. The coupling of F_2 with the dark photon will be modified by the charge ratio: $Z' \equiv Q'_{F_2} / Q'_{F_1}$. By means of a nonorthogonal transformation, one can remove the kinetic mixing and show that the net effect of the relevant term is to provide the dark fermions with a tiny ordinary electric charge [20]. The physical photon now couples to dark fermions with charge,

$$\cos\theta_w g' Q'_{F_j} \epsilon' \equiv \epsilon_{F_j} e. \qquad (3)$$

Thus the fundamental physics of the model is described by five independent parameters: $m_{F_1}, m_{F_2}, \alpha', Z'$ and $\epsilon \equiv \epsilon_{F_1}$ (note that $\epsilon_{F_2} = Z' \epsilon_{F_1}$ and is therefore not an independent parameter). For definiteness we will focus on the case $m_{F_1} \ll m_{F_2}$, with Z' being an integer.

Clearly it is entirely possible for our model to be the low energy effective field theory limit of a more complex theory. In this context, F_1 and/or F_2 might represent bound states (dark nuclei), which could be bound together by some interaction which resembles the strong one. In this case, the F_1/F_2 masses arise from a dark confinement scale (analogous to Λ_{QCD} in the Standard Model) rather than being a bare mass term. Alternatively, the mass terms for F_j might originate from a hidden sector scalar, S, by means of a Lagrangian term of the form $\lambda_j S \bar{F}_j F_j$, with $\langle S \rangle \neq 0$.

Some possible implications of this model for dark matter direct detection experiments have been discussed previously in [21]. Furthermore, as explained in the

Introduction, the dark matter phenomenology is similar but generalizes the MDM case. Related hidden sector models, featuring an unbroken $U(1)'$ interaction, have also been discussed in recent literature, e.g. [4,5,22] and much earlier in [23]. However, these models assume parameter space where the dark matter galactic halo is in the form of atoms (or a nondissipative plasma), and thus can be collisional but generally not dissipative.[2] We consider the case where the galactic halo is in the form of a roughly spherical dissipative plasma. Such a spherical plasma would cool via dissipative processes, for instance dark bremsstrahlung, unless a substantial heat source exists. Here a pivotal role is played by the kinetic mixing interaction: kinetic mixing induced processes (such as plasmon decay [25,26]) within the core of ordinary core-collapse supernovae are presumed to provide the heat source that replaces the energy lost to dissipative interactions. This is possible provided $\epsilon \sim 10^{-9}$ and $m_{F_1} \lesssim$ few $\times T_{SN} \simeq 100$ MeV, where T_{SN} is the temperature reached in the core of ordinary supernovae.[3] A lower limit $m_{F_1} \gtrsim 0.01$ MeV arises from studies of red giants [29] and white dwarfs [26,30] (see [31] for a summary of relevant bounds).

Finally, one can also consider a two-component hidden sector model where the two dark matter particles are bosons rather than fermions, charged under a $U(1)'$ gauge interaction. In the case of two scalar particles, B_j, the Lagrangian is

$$\mathcal{L} = \mathcal{L}_{SM} - \frac{1}{4}F'^{\mu\nu}F'_{\mu\nu} + (D_\mu B_j)^\dagger (D^\mu B_j)$$
$$- m_{B_j}^2 B_j^\dagger B_j - \frac{\epsilon'_B}{2}F^{\mu\nu}F'_{\mu\nu}, \qquad (4)$$

where $j = 1, 2$ (with summation over j implied). As in the two-component fermion case, one can consider the general case where the $U(1)'$ charges of B_1 and B_2 are different, with Z'_B being the charge ratio. As before, the Lagrangian in Eq. (4) possesses an accidental global $U(1)$ symmetry[4] which together with the $U(1)'$ gauge symmetry implies conservation of B_1 and B_2 numbers, and hence stability of

the dark matter particles. Again, the kinetic mixing term will play a dominant role in the cosmological and galactical dynamics of such a model. Barring factors of order unity to account for spin statistics, the analysis we will perform in the following sections will hold for this bosonic model as well as the fermionic one. In particular, the bounds that are summarized in Sec. VI hold for the bosonic case, up to factors of order unity. For definiteness, though, we will focus on the fermionic model.

III. COSMOLOGY OF THE EARLY UNIVERSE

In SecS. III and IV we derive constraints on the parameter space of the model from early universe cosmology considerations. We assume at the outset that the light F_1 particle has mass in the range 0.01 MeV $\lesssim m_{F_1} \lesssim$ 100 MeV. As mentioned in the previous section, and discussed in more detail in Sec. V, this mass range for the F_1 particle is motivated by the adopted dissipative dynamics governing galactic halos, which sees substantial halo heating from ordinary core-collapse supernovae compensating for the energy lost due to dissipative interactions. This mechanism also requires kinetic mixing of magnitude $\epsilon \sim 10^{-9}$ which, it turns out, is in the interesting range where it can be probed by early universe cosmology.

A. Evolution of $\frac{T_{\gamma_D}}{T_\gamma}$

Successful cosmology, BBN and LSS strongly constrain exotic contributions to the energy density during the radiation dominated era. If we define $T_\gamma[T_{\gamma_D}]$ and T_ν to be the photon [dark photon] and neutrino temperatures, then we require $T_{\gamma_D} \ll T_\gamma$ (the exact mechanism that provides such an initial condition will not be of our concern, although asymmetric reheating is possible within inflationary models [32]).[5] As discussed previously, kinetic mixing confers a tiny ordinary electric charge to dark fermions. It follows that in the early universe energy and entropy can be transferred between the sectors. Thus even if the Universe starts with $T_{\gamma_D}/T_\gamma = 0$, T_{γ_D} will be generated as entropy is transferred from the visible to the hidden sector. In the following work we first study the evolution of T_{γ_D}/T_γ (with initial condition $T_{\gamma_D}/T_\gamma = 0$), and then consider the relevant cosmological constraints.

In the early universe energy is transferred between the sectors via various processes, including (to order ϵ^2) $e\bar{e} \to F_1\bar{F}_1$, $eF_1 \to eF_1$, $e\bar{e} \to F_2\bar{F}_2$, and $\gamma F_1 \to \gamma_D F_1$. Given the assumed initial condition, $T_{\gamma_D}/T_\gamma = 0$, we can to

---

[2]An alternative possibility examined in recent literature, known as double-disk dark matter (DDDM), explores the scenario where only a subdominant component of the dark matter exhibits dissipative interactions [24]. These dissipative dynamics allow for DDDM to cool efficiently and form a thin dark matter disk, similar to the baryonic disk.

[3]Although the kinetic mixing parameter is very small, $\epsilon \sim 10^{-9}$, this does not represent a theoretical problem, such as radiative instability. Indeed, as discussed in [27], small values for the coupling are technically natural (in the sense of 't Hooft [28]) since, in the limit $\epsilon \to 0$, an enhanced Poincaré symmetry arises: $\mathcal{G}_P^{SM} \otimes \mathcal{G}_P^{HS}$, where $\mathcal{G}_P$ denotes the Poincaré group and SM and HS stand for Standard Model and hidden sector, respectively.

[4]Technically, this accidental global $U(1)$ symmetry will be present only if the $U(1)'$ charges of B_1 and B_2 are such as to prevent interaction terms like $\lambda B_1^3 B_2$.

[5]We only require $T_{\gamma_D} \ll T_\gamma$ at, say, the QCD phase transition, $T_{QCD} \sim 100$ MeV. Thus, even if the Universe started with $T_{\gamma_D} = T_\gamma$ at $T > T_{QCD}$, the heating of the ordinary sector at the QCD phase transition would be sufficient to establish the necessary initial condition, $T_{\gamma_D} \ll T_\gamma$, at T_{QCD}.

a reasonable approximation neglect inverse processes, such as $F_1 \bar{F}_1 \rightarrow e\bar{e}$. Also, processes involving F_2 can be approximately neglected if F_2 is much heavier than F_1 [simple analytic calculations indicate that for $m_{F_2} \gg Z'^2 \max(m_e, m_{F_1})$ the energy transfer between the sectors is dominated by F_1 production]. Of the remaining processes, $e\bar{e} \rightarrow F_1 \bar{F}_1$ is expected to dominate (for $T_\gamma \gtrsim m_e$), given that the rates of all other two-body processes are smaller by a factor of $\lesssim n_{F_1}/n_e \sim (T_{\gamma_D}/T_\gamma)^3$, and typically we are constrained to reside in the region of parameter space where $(T_{\gamma_D}/T_\gamma)^3 \ll 1$. Hence for $m_{F_1} \gtrsim 0.1$ MeV, we consider just one production process, $e\bar{e} \rightarrow F_1 \bar{F}_1$.[6]

For $m_{F_1} \lesssim 0.1$ MeV, one could consider processes such as $\gamma F_1 \rightarrow \gamma_D F_1$ in addition to $e\bar{e} \rightarrow F_1 \bar{F}_1$. Although the rate for $\gamma F_1 \rightarrow \gamma_D F_1$ is suppressed relative to $e\bar{e} \rightarrow F_1 \bar{F}_1$ by $\sim(T_{\gamma_D}/T_\gamma)^3$ for $T_\gamma \gtrsim m_e$, for $T_\gamma \lesssim m_e$ the rate of $\gamma F_1 \rightarrow \gamma_D F_1$ can become important and eventually dominate.[7] Here we shall focus on $m_{F_1} \gtrsim 0.1$ MeV, where $e\bar{e} \rightarrow F_1 \bar{F}_1$ is the dominant process affecting the evolution of the temperatures. Thus, our analysis will only be strictly valid in the range 0.1 MeV $\lesssim m_{F_1} \lesssim$ 100 MeV, while the study of the region 0.01 MeV $\lesssim m_{F_1} \lesssim$ 0.1 MeV will require further work. Restricting ourselves to the region of parameter space $m_{F_1} \gtrsim 0.1$ MeV also bypasses several other complications which arise in the context of galactic structure (Sec. V).

The cross section for $e\bar{e} \rightarrow F_1 \bar{F}_1$ is analogous to that of muon pair production, with the essential difference being that the coupling of F_1 to the ordinary photon is now given by ϵe. The cross section for this process is

$$\sigma = \frac{4\pi}{3s^3} \epsilon^2 \alpha^2 \sqrt{\frac{s - 4m_{F_1}^2}{s - 4m_e^2}} [s^2 + 2(m_e^2 + m_{F_1}^2)s + 4m_e^2 m_{F_1}^2],$$

(5)

where $\sqrt{s}$ is the center-of-momentum energy of the system, $\alpha = e^2/4\pi$ is the fine-structure constant and m_e is the electron mass. The following treatment generalizes the MDM case analyzed in [34], which itself followed earlier

---

[6]While this work was in progress, a paper [33] appeared which considered N_{eff} constraints on a related model. There they considered additional production channels, such as $\gamma F_1 \rightarrow \gamma_D F_1$, for a wide range of parameter space. The effect of these extra channels is to tighten constraints on ϵ by around a factor of 2.

[7]Another F_1 production channel that could be relevant for very low F_1 mass is plasmon decay ($\gamma \rightarrow F_1 \bar{F}_1$). It can become important when $m_{F_1} \lesssim \omega_P/2$, where $\omega_P = \sqrt{4\pi\alpha T^2/9}$ is the plasma frequency (see e.g. [26]). This implies that during the period of interest (from BBN to the formation of the CMB) plasmon decay is only important for $m_{F_1} \lesssim 50$ keV.

works [26,35,36]. Energy is transferred between the visible and dark sectors within a comoving volume R^3 (R being the scale factor) at a rate given by

$$\frac{dQ}{dt} = R^3 n_e n_{\bar{e}} \langle \sigma v_{\text{Møl}} \mathcal{E} \rangle,$$

(6)

where $\langle \sigma v_{\text{Møl}} \mathcal{E} \rangle$ denotes the thermal average of the cross section (σ), the Møller velocity ($v_{\text{Møl}}$) and the total energy of the process ($\mathcal{E} = E_1 + E_2$). Following [36,37], we replace the exact Fermi-Dirac distribution with the simpler Maxwellian one, so that the thermally averaged cross section is given by

$$\langle \sigma v_{\text{Møl}} \mathcal{E} \rangle = \frac{\int d^3 p_1 d^3 p_2 e^{-\frac{E_1}{T}} e^{-\frac{E_2}{T}} \sigma v_{\text{Møl}} \mathcal{E}}{\int d^3 p_1 d^3 p_2 e^{-\frac{E_1}{T}} e^{-\frac{E_2}{T}}}.$$

(7)

To evaluate the thermally averaged cross section, similar steps as in [36,37] can be followed, yielding

$$\langle \sigma v_{\text{Møl}} \mathcal{E} \rangle = \frac{\omega}{8m_e^4 T_\gamma^2 [K_2(\frac{m_e}{T_\gamma})]^2} \int_{4\mathcal{M}^2}^\infty ds \sigma(s - 4m_e^2)$$

$$\times \sqrt{s} \int_{\sqrt{s}}^\infty dE_+ e^{-\frac{E_+}{T_\gamma}} E_+ \sqrt{\frac{E_+^2}{s} - 1},$$

(8)

where $\omega \approx 0.8$ takes into account various approximations such as the aforementioned use of a Maxwell-Boltzmann distribution in lieu of the actual Fermi-Dirac one in evaluating the thermally averaged cross section [36]. $K_2(z)$ is the modified Bessel function of the second kind and argument z, and $\mathcal{M} \equiv \max(m_e, m_{F_1})$. Finally, we can write (see for instance [38])

$$n_e \simeq n_{\bar{e}} = \frac{1}{\pi^2} \int_{m_e}^\infty dE \frac{\sqrt{E^2 - m_e^2} E}{1 + e^{\frac{E}{T_\gamma}}}.$$

(9)

Since self-interaction rates are bigger than the rates of kinetic mixing induced processes by many orders of magnitude ($\sim 1/\epsilon^2$), the overall system can be modeled as being composed of two subsystems, one at temperature T_γ and the other at temperature T_{γ_D}, exchanging energy while remaining instantaneously in thermodynamical equilibrium. This system is somewhat analogous to that of a block of ice melting in a glass of water (e.g. [39]). The second law of thermodynamics can therefore be applied to it. In principle, the neutrino subsystem should be taken into account too. In practice the net transfer of energy to the neutrino subsystem can be approximately neglected, at least for $m_{F_1} \lesssim 10$ MeV, since energy transfer to the dark sector then happens predominantly after neutrino kinetic

decoupling.[8] This means that $dS_\nu \simeq 0$. Nevertheless, the evolution of T_ν will still have to be taken into account, though it trivially scales as the inverse of the scale factor (see e.g. [38]).

The second law of thermodynamics states that the change in entropy in the visible sector is given by

$$dS = -\frac{dQ}{T_\gamma}. \tag{10}$$

Similarly, the change in entropy for the dark sector is

$$dS' = \frac{dQ}{T_{\gamma_D}}. \tag{11}$$

A useful way to express the entropy of a particle species in cosmology is given in e.g. [38]

$$S = \frac{\rho + p}{T} R^3, \tag{12}$$

where ρ, p and T denote its energy density, pressure and temperature, respectively. Taking the derivative with respect to time on both sides of Eqs. (10) and (11) and combining the result with Eqs. (6) and (12) yields

$$\frac{d}{dt}\left[\frac{(\rho_\gamma + p_\gamma + \rho_e + p_e)R^3}{T_\gamma}\right] = -\frac{n_e n_{\bar{e}}\langle \sigma v_{\text{Møl}}\mathcal{E}\rangle R^3}{T_\gamma},$$
$$\frac{d}{dt}\left[\frac{(\rho_{\gamma_D} + p_{\gamma_D} + \rho_{F_1} + p_{F_1})R^3}{T_{\gamma_D}}\right] = \frac{n_e n_{\bar{e}}\langle \sigma v_{\text{Møl}}\mathcal{E}\rangle R^3}{T_{\gamma_D}}, \tag{13}$$

where we have neglected the neutrino contribution to the entropy change, which is justified as $dS_\nu \simeq 0$, as discussed above. In Eqs. (13) and below, we have defined $\rho_e \equiv \rho_e + \rho_{\bar{e}}$, and similarly for p_e, ρ_{F_1} and p_{F_1}.

The ^{00} component of the Einstein field equations for the FRW metric describes the evolution of the scale factor R. This is known as the first Friedmann equation and in a flat universe takes the form

---

[8]For F_1 masses in the range 10 MeV $\lesssim m_{F_1} \lesssim$ 100 MeV, there can be a significant transfer of entropy out of the neutrino subsystem. For the largest F_1 masses, $m_{F_1} \sim$ 100 MeV, the evolution can be separated into two distinct stages. The first is where $F_1, \bar{F}_1$ states are produced via processes such as $\bar{e}e \to \bar{F}_1 F_1$. For these largest F_1 masses of interest, these production processes will only be important for temperatures above the kinetic decoupling of the neutrinos so that $T_\nu = T_\gamma$ results. The second stage is the annihilation of electrons and positrons ($\bar{e}e \to \gamma\gamma$) which continues to occur at temperatures where the neutrinos have kinetically decoupled and leads to the heating of photons relative to the neutrinos ($T_\gamma > T_\nu$). We have checked that the effect of neglecting the transfer of entropy to the neutrino system during the $F_1, \bar{F}_1$ production era does not greatly modify ($\lesssim$20%) our derived limits on ϵ from the constraints on δN_{eff}.

$$\left(\frac{\dot{R}}{R}\right)^2 = \frac{8\pi G_N}{3}[\rho_\gamma + \rho_e + \rho_\nu + \rho_{\gamma_D} + \rho_{F_1}]. \tag{14}$$

Defining $x \equiv m_e/T_\gamma$, energy densities and pressures in the visible sector are given in e.g. [38]

$$\rho_\gamma = \frac{\pi^2}{15} T_\gamma^4,$$
$$p_\gamma = \frac{\pi^2}{45} T_\gamma^4,$$
$$\rho_e = \frac{2T_\gamma^4}{\pi^2} \int_x^\infty du \frac{(u^2 - x^2)^{\frac{1}{2}} u^2}{1 + e^u},$$
$$p_e = \frac{2T_\gamma^4}{3\pi^2} \int_x^\infty du \frac{(u^2 - x^2)^{\frac{3}{2}}}{1 + e^u},$$
$$\rho_\nu = \frac{7\pi^2}{40} T_\nu^4. \tag{15}$$

Similarly for the dark sector, with $x' \equiv m_{F_1}/T_{\gamma_D}$,

$$\rho_{\gamma_D} = \frac{\pi^2}{15} T_{\gamma_D}^4,$$
$$p_{\gamma_D} = \frac{\pi^2}{45} T_{\gamma_D}^4,$$
$$\rho_{F_1} = \frac{2T_{\gamma_D}^4}{\pi^2} \int_{x'}^\infty du \frac{(u^2 - x'^2)^{\frac{1}{2}} u^2}{1 + e^u},$$
$$p_{F_1} = \frac{2T_{\gamma_D}^4}{3\pi^2} \int_{x'}^\infty du \frac{(u^2 - x'^2)^{\frac{3}{2}}}{1 + e^u}. \tag{16}$$

Considering the neutrino subsystem, the neutrino temperature scales as $T_\nu \propto 1/R$ which follows from $dS_\nu \simeq 0$. Noting that all proportionality factors cancel [being there the same power of the scale factor R on both sides of Eqs. (13)], R in Eqs. (13) can effectively be replaced by $1/T_\nu$. Accordingly, Eqs. (13) can be expressed as

$$\frac{d}{dt}\left[\frac{(\rho_\gamma + p_\gamma + \rho_e + p_e)}{T_\gamma T_\nu^3}\right] = -\frac{n_e n_{\bar{e}}\langle \sigma v_{\text{Møl}}\mathcal{E}\rangle}{T_\gamma T_\nu^3},$$
$$\frac{d}{dt}\left[\frac{(\rho_{\gamma_D} + p_{\gamma_D} + \rho_{F_1} + p_{F_1})}{T_{\gamma_D} T_\nu^3}\right] = \frac{n_e n_{\bar{e}}\langle \sigma v_{\text{Møl}}\mathcal{E}\rangle}{T_{\gamma_D} T_\nu^3}, \tag{17}$$

and Eq. (14) as

$$\frac{1}{T_\nu}\frac{dT_\nu}{dt} = -\sqrt{\frac{8\pi G_N}{3}(\rho_\gamma + \rho_e + \rho_\nu + \rho_{\gamma_D} + \rho_{F_1})}. \tag{18}$$

Some manipulation shows that Eqs. (17) can be brought to the form

$$\zeta \frac{dT_\gamma}{dt} + \kappa \frac{dT_\nu}{dt} = -\frac{n_e n_{\bar{e}} \langle \sigma v_{\text{Møl}} \mathcal{E} \rangle}{T_\gamma^3},$$

$$\zeta' \frac{dT_{\gamma_D}}{dt} + \kappa' \frac{dT_\nu}{dt} = \frac{n_e n_{\bar{e}} \langle \sigma v_{\text{Møl}} \mathcal{E} \rangle}{T_{\gamma_D}^3}, \quad (19)$$

where

$$\zeta \equiv \frac{3\rho_\gamma}{T_\gamma^4} + \frac{3p_\gamma}{T_\gamma^4} + \frac{3\rho_e}{T_\gamma^4} + \frac{3p_e}{T_\gamma^4}$$
$$+ \frac{2m_e^2}{\pi^2 T_\gamma^2} \int_x^\infty du \frac{(u^2 - x^2)^{-\frac{1}{2}} u^2 + (u^2 - x^2)^{\frac{1}{2}}}{1 + e^u},$$

$$\kappa \equiv -\left(\frac{3\rho_\gamma}{T_\gamma^3} + \frac{3p_\gamma}{T_\gamma^3} + \frac{3\rho_e}{T_\gamma^3} + \frac{3p_e}{T_\gamma^3} \right) \frac{1}{T_\nu},$$

$$\zeta' \equiv \frac{3\rho_{\gamma_D}}{T_{\gamma_D}^4} + \frac{3p_{\gamma_D}}{T_{\gamma_D}^4} + \frac{3\rho_{F_1}}{T_{\gamma_D}^4} + \frac{3p_{F_1}}{T_{\gamma_D}^4}$$
$$+ \frac{2m_{F_1}^2}{\pi^2 T_{\gamma_D}^2} \int_{x'}^\infty du \frac{(u^2 - x'^2)^{-\frac{1}{2}} u^2 + (u^2 - x'^2)^{\frac{1}{2}}}{1 + e^u},$$

$$\kappa' \equiv -\left(\frac{3\rho_{\gamma_D}}{T_{\gamma_D}^3} + \frac{3p_{\gamma_D}}{T_{\gamma_D}^3} + \frac{3\rho_{F_1}}{T_{\gamma_D}^3} + \frac{3p_{F_1}}{T_{\gamma_D}^3} \right) \frac{1}{T_\nu}. \quad (20)$$

We are now left with a closed system of three differential equations [Eqs. (18) and (19)] for three unknowns $(T_\gamma, T_{\gamma_D}$ and $T_\nu)$. Given suitable initial conditions, then, the system can be solved numerically to give the evolution of these three quantities. An example is presented in Fig. 1, where the evolution of T_{γ_D}/T_γ is plotted as a function of T_γ for different values of m_{F_1} and for $\epsilon = 10^{-9}$. Note that the flow of time is from the right to the left.

It can be seen from Fig. 1 that T_{γ_D}/T_γ asymptotically approaches a constant at late times. We would like to find an approximate analytic expression for the asymptotic value of T_{γ_D}/T_γ. It is perhaps useful to recall the results
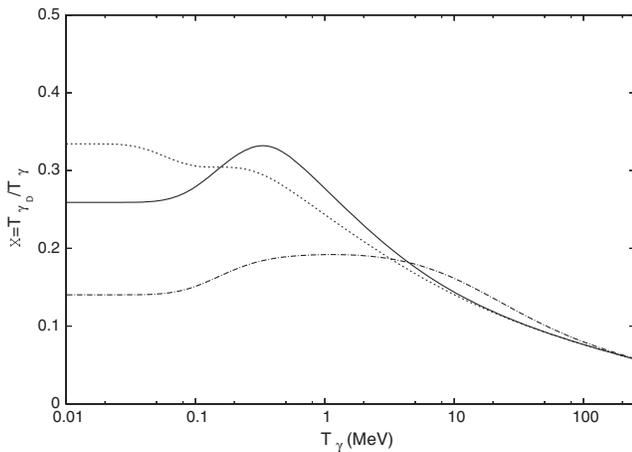

FIG. 1. Evolution of $\mathcal{X} \equiv T_{\gamma_D}/T_\gamma$ for $m_{F_1} = 10$ MeV (dot-dashed line), $m_{F_1} = 1$ MeV (solid line) and $m_{F_1} = 0.1$ MeV (dashed line).

obtained for MDM. In this context, MDM can be viewed as a special case of our model in the limit where $m_{F_1} = m_e$. For the case of MDM it has been found that $T_{\gamma'}/T_\gamma$ (where γ' denotes the mirror photon, which is of course analogous to our dark photon, γ_D) asymptotically evolves to [34]

$$\frac{T_{\gamma'}}{T_\gamma} \simeq 0.31 \left(\frac{\epsilon}{10^{-9}} \right)^{\frac{1}{2}}. \quad (21)$$

More generally, $m_{F_1} \neq m_e$ in the context of our two-component hidden sector model, and one expects a somewhat different behavior in T_{γ_D}/T_γ to account for this m_{F_1} dependence. Previous work in the MDM context shows that in the limit of $T_\gamma \gg m_e$, an analytic expression can be found for $T_{\gamma'}/T_\gamma$ [36],

$$\frac{T_{\gamma'}}{T_\gamma} \propto \sqrt{\epsilon} \left[\frac{1}{T} - \frac{1}{T_i} \right]^{\frac{1}{4}}, \quad (22)$$

with an assumed initial condition $T_{\gamma'} = 0$ at $T_\gamma = T_i$. For $T_\gamma \sim m_e$, energy transfer to the mirror sector cuts off, as the process $e\bar{e} \rightarrow e'\bar{e}'$ becomes infrequent due to Boltzmann suppression of e, $\bar{e}$ number densities.

We can attempt to generalize the result to our case. The process $e\bar{e} \rightarrow F_1 \bar{F}_1$ will cease to be important at temperatures below $\sim \mathcal{M} \equiv \max(m_e, m_{F_1})$. Equation (22) then suggests that the asymptotic value of the ratio T_{γ_D}/T_γ is proportional to $\sqrt{\epsilon}(m_e/\mathcal{M})^{\frac{1}{4}}$. This intuition has been verified numerically, by evolving for different values of ϵ and m_{F_1}. Numerically, we find that the asymptotic value of T_{γ_D}/T_γ can be expressed in the form

$$\frac{T_{\gamma_D}}{T_\gamma} \simeq 0.31 \sqrt{\frac{\epsilon}{10^{-9}}} \left(\frac{m_e}{\mathcal{M}} \right)^{\frac{1}{4}},$$
$$\mathcal{M} \equiv \max(m_e, m_{F_1}), \quad (23)$$

for parameters in the range $\epsilon \sim 10^{-9}$ and 0.1 MeV $\lesssim m_{F_1} \lesssim 100$ MeV.

One can also attempt to understand the shape of the curves in Fig. 1. At early times $(T_\gamma \gg m_{F_1}, m_e)$ the curves overlap, following a $T_{\gamma_D}/T_\gamma \propto (1/T_\gamma)^{\frac{1}{4}}$ behavior consistent with the analytic solution previously discussed. At some later time corresponding to $T_\gamma \sim \mathcal{M}$, the curves start deviating from the analytic solution. The rising of the various curves at different temperatures and with characteristic bumps can be understood in terms of annihilation processes which are heating the respective sectors roughly at the temperature corresponding to the mass of the particle-antiparticle pair which is annihilating. That is, electron-positron and F_1-$\bar{F}_1$ annihilations explain the deviation of the numerical solution from the simpler analytic one. Once the annihilation processes are over, T_{γ_D}/T_γ reaches its asymptotic value.

B. Calculation of $\delta N_{\text{eff}}[\text{CMB}]$

We now compute the modification of the energy density at the hydrogen recombination epoch in the early universe. A way to parametrize this extra energy density is in terms of an effective number of neutrino species. Recall that the relativistic energy density component at recombination can be expressed as

$$\rho_{\text{rad}} = \left(1 + \frac{7}{8}\left(\frac{4}{11}\right)^{\frac{4}{3}} N_{\text{eff}}[\text{CMB}]\right)\rho_\gamma, \qquad (24)$$

where the factor of $7/8$ takes into account the different statistical natures (fermionic instead of bosonic) of neutrinos with respect to photons, and the factor of $4/11$ takes care of γ heating due to $e\bar{e}$ annihilation after neutrino kinetic decoupling (see for instance [38]). N_{eff} is referred to as the effective number of neutrinos and is predicted to be $N_{\text{eff}} \simeq 3.046$ in the Standard Model (see e.g. [40]). Observations from WMAP [41], the South Pole Telescope [42], the Atacama Cosmology Telescope [43] and the Planck mission [44] are consistent with the Standard Model predictions and can be used to constrain $\delta N_{\text{eff}}[\text{CMB}] \equiv N_{\text{eff}}[\text{CMB}] - 3.046$. Using the result of Planck's analysis $N_{\text{eff}}[\text{CMB}] = 3.30 \pm 0.27$ [44] gives the 2σ upper limit: $\delta N_{\text{eff}}[\text{CMB}] < 0.80$.

In our model the modification to the effective number of neutrinos can be written as follows:

$$\delta N_{\text{eff}}[\text{CMB}] = 3\left(\left[\frac{T_\nu(\epsilon)}{T_\nu(\epsilon = 0)}\right]^4 - 1\right) + \frac{8}{7}\left(\frac{T_{\gamma_D}(\epsilon)}{T_\nu(\epsilon = 0)}\right)^4,$$
$$(25)$$

where the temperatures are evaluated at photon decoupling, $T_\gamma \simeq 0.26$ eV. The two terms on the right-hand side of Eq. (25) account for distinct effects. First, the process $e\bar{e} \to F_1\bar{F}_1$ will increase T_{γ_D} at the expense of T_γ, thus reducing T_γ/T_ν and effectively increasing the number of neutrino species at recombination. The second term is the direct increase in $N_{\text{eff}}[\text{CMB}]$ due to the increase in T_{γ_D} itself.

One has to pay attention when using $\delta N_{\text{eff}}[\text{CMB}]$ to set constraints on the parameter space, since the addition of energy density is not the only effect to consider. Prior to the recombination of F_1 and F_2 into neutral dark states, dark matter behaves like a tightly coupled fluid, analogous to the photon-baryon fluid in the visible sector. This fluid undergoes acoustic oscillations, which suppress power on small scales, hence behaving very differently from collisionless CDM. Thus, there are two quite different possible effects for the CMB to consider. The first is the extra energy density as parametrized by $\delta N_{\text{eff}}[\text{CMB}]$, and the second is the effect of dark acoustic oscillations prior to dark recombination. In this section we consider the energy density modification, while the constraints arising from dark acoustic oscillations will be dealt with in Sec. IV.
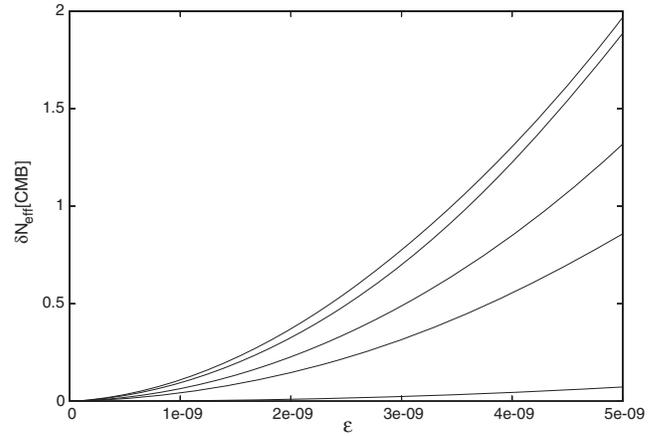

FIG. 2. $\delta N_{\text{eff}}[\text{CMB}]$ versus ϵ at fixed values of m_{F_1} for (going from up to down) $m_{F_1} = 0.1, 0.511, 0.7, 1, 10$ MeV.

In Fig. 2, we present results for $\delta N_{\text{eff}}[\text{CMB}]$ obtained by numerically solving Eq. (25) [in the process, solving also Eqs. (18) and (19)] for some example parameter choices. We set constraints on our model by using the limit $\delta N_{\text{eff}}[\text{CMB}] < 0.80$. In Fig. 3 the exclusion limits for our model in the ϵ-m_{F_1} parameter space are shown, with the excluded region being above the line. Notice for $m_{F_1} = 0.511$ MeV we recover the bound on ϵ obtained for MDM, $\epsilon \lesssim 3.5 \times 10^{-9}$ [34].

C. Calculation of $\delta N_{\text{eff}}[\text{BBN}]$

The addition of extra energy density during the early universe also has an effect on BBN, the process during which light nuclei, and in particular helium, were synthesized (for a more detailed review see e.g. [45]). It is known that increasing the energy density by the addition of one neutrino species increases the helium fraction, Y_p, by approximately 0.013 [46]. It follows therefore that the change in the effective number of neutrino species associated with BBN is approximately given by
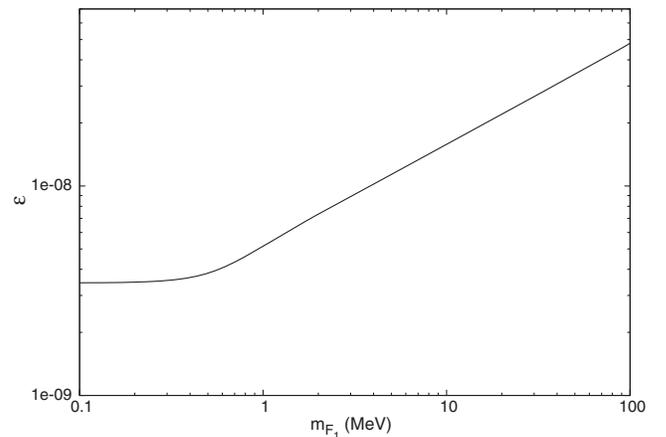

FIG. 3. Exclusion limits obtained from $\delta N_{\text{eff}}[\text{CMB}] < 0.80$ in ϵ-m_{F_1} parameter space (excluded region is above line).

$$\delta N_{\text{eff}}[\text{BBN}] = \frac{Y_p(\epsilon) - Y_p(\epsilon = 0)}{0.013}. \qquad (26)$$

The first step toward the synthesis of helium is the synthesis of deuterium which, in turn, depends on the neutron abundance $X_n \equiv n_p/(n_n + n_p)$. We begin by considering the weak interaction processes which affect the neutron abundance,

$$n + \nu_e \leftrightarrow p + e,$$
$$n + \bar{e} \leftrightarrow p + \bar{\nu}_e,$$
$$n \rightarrow p + e + \bar{\nu}_e. \qquad (27)$$

At equilibrium (hence, at high temperatures) $X_n \simeq 1/(1 + e^{Q/T})$, where $Q \simeq 1.293$ MeV is the difference between the neutron and the proton masses.

The rates for the four processes which affect the neutron abundance (excluding neutron decay) can be found in e.g. [45]

$$\lambda_1 \equiv \lambda(n + \nu_e \rightarrow p + e)$$
$$= A \int_0^\infty dP_\nu E_e^2 P_\nu^2 \frac{1}{e^{\frac{E_\nu}{T_\nu}} + 1} \frac{1}{e^{-\frac{E_e}{T_\gamma}} + 1},$$

$$\lambda_2 \equiv \lambda(n + \bar{e} \rightarrow p + \bar{\nu}_e)$$
$$= A \int_0^\infty dP_e E_\nu^2 P_e^2 \frac{1}{e^{\frac{E_e}{T_\gamma}} + 1} \frac{1}{e^{-\frac{E_\nu}{T_\nu}} + 1},$$

$$\lambda_3 \equiv \lambda(p + e \rightarrow n + \nu_e)$$
$$= A \int_{\sqrt{Q^2 - m_e^2}}^\infty dP_e E_\nu^2 P_e^2 \frac{1}{e^{\frac{E_e}{T_\gamma}} + 1} \frac{1}{e^{-\frac{E_\nu}{T_\nu}} + 1},$$

$$\lambda_4 \equiv \lambda(p + \bar{\nu}_e \rightarrow n + \bar{e})$$
$$= A \int_{Q + m_e}^\infty dP_\nu E_e^2 P_\nu^2 \frac{1}{e^{\frac{E_\nu}{T_\nu}} + 1} \frac{1}{e^{-\frac{E_e}{T_\gamma}} + 1}, \qquad (28)$$

where $E_e[E_\nu]$, $P_e[P_\nu]$ indicate the electron [neutrino] energy and momentum, respectively. The extremals of the integrals are obtained from kinematical considerations. The factors within the integrals account for Fermi-Dirac statistics and Pauli blocking. The values of the various constants are given by

$$A = \frac{G_F^2(1 + 3g_A^2)\cos^2\theta_c}{2\pi^3},$$
$$G_F = 1.166 \times 10^{-5} \text{ GeV}^{-2},$$
$$g_A = 1.257,$$
$$\cos\theta_c = 0.97456. \qquad (29)$$

The evolution of the neutron abundance, X_n, is governed by the differential equation,

$$\frac{dX_n}{dt} = -(\lambda_1 + \lambda_2 + \lambda_n)X_n + (\lambda_3 + \lambda_4)(1 - X_n), \qquad (30)$$

where $\lambda_n^{-1} = \tau_n \simeq 886.7$ s is the neutron lifetime. Equation (30) can be used to evolve the neutron fraction down to the so-called *deuterium bottleneck* temperature $T_\gamma \simeq 0.07$ MeV [of course, Eqs. (18) and (19) need to be solved simultaneously to obtain the modified time-temperature relation]. The helium fraction, Y_p, is twice the value of X_n at this time, and $\delta N_{\text{eff}}[\text{BBN}]$ can be evaluated by using Eq. (26).

There are hints that $\delta N_{\text{eff}}[\text{BBN}]$ is also nonzero and positive. The data constrain $\delta N_{\text{eff}}[\text{BBN}] < 1$ at around 95% confidence level [47]. In Fig. 4 $\delta N_{\text{eff}}[\text{BBN}]$ is plotted against ϵ keeping m_{F_1} fixed. The constraints following from this analysis are shown together with those obtained from $\delta N_{\text{eff}}[\text{CMB}]$ in Fig. 5. Evidently the limits set by $\delta N_{\text{eff}}[\text{CMB}]$ are more stringent than those set by $\delta N_{\text{eff}}[\text{BBN}]$. Finally, we find an analytic approximation
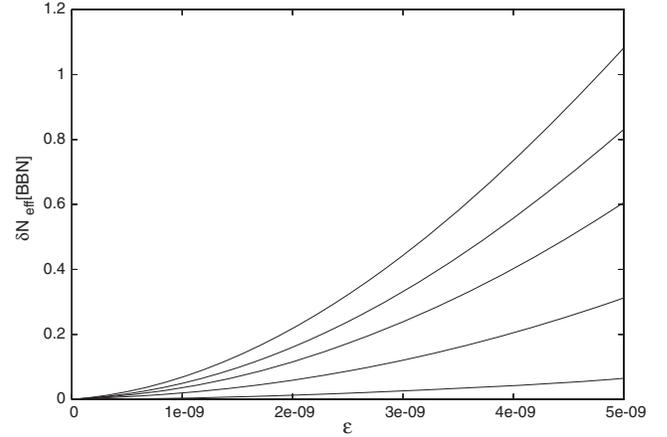

FIG. 4. $\delta N_{\text{eff}}[\text{BBN}]$ versus ϵ at fixed values of m_{F_1} for (going from up to down) $m_{F_1} = 0.1, 0.7, 1, 2, 10$ MeV.
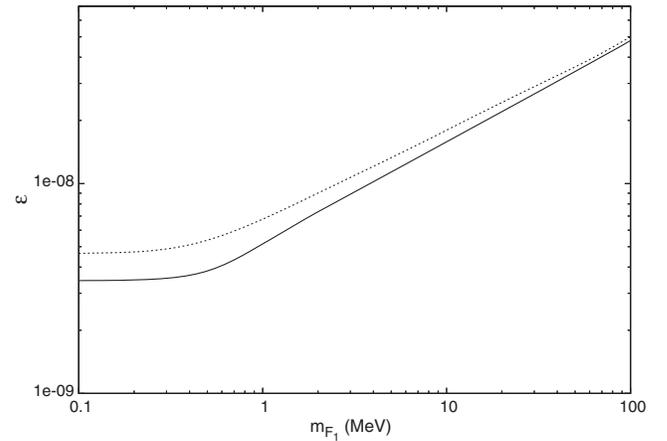

FIG. 5.   Exclusion limits from $\delta N_{\text{eff}}[\text{CMB}] < 0.80$ (solid line) and $\delta N_{\text{eff}}[\text{BBN}] < 1$ (dashed line). Regions above lines are excluded.

to CMB δN_{eff} constraints on ϵ arising from early universe cosmology,

$$\epsilon \lesssim 3.5 \times 10^{-9} \left(\frac{\mathcal{M}}{m_e} \right)^{\frac{1}{2}}. \qquad (31)$$

The $\epsilon \sim \mathcal{M}^{\frac{1}{2}}$ dependence can easily be understood by referring to Eqs. (23) and (25).

IV. DARK RECOMBINATION

A. Saha equation for dark recombination

Additional energy density, as parametrized by $\delta N_{\text{eff}}[\text{CMB}]$, is not the only new physics affecting the CMB. Prior to recombination of F_1 and F_2 into neutral dark states, dark matter behaves like a tightly coupled fluid which undergoes dark acoustic oscillations. These oscillations suppress power on small scales (hence deviating from collisionless CDM), below some characteristic scale $L^\star$, which is itself a function of the parameters in our model. Ultimately such a suppression of power on small scales may help in explaining the observed dearth of small galaxies in the neighborhood of the Milky Way. In the following, though, we simply derive approximate bounds by requiring that $T_{\text{dr}} \gtrsim T_{\text{eq}}$, where T_{dr} is the temperature in the visible sector at the time of *dark recombination*, and T_{eq} is the temperature of matter-radiation equality. This requirement has been used in the literature (see for instance [48]), and follows from studies in the MDM context [9,49,50]. Roughly, $T_{\text{dr}} \gtrsim T_{\text{eq}}$ means that LSS is unaffected by dark acoustic oscillations on scales which are still growing linearly today.

In the present model, *dark recombination* involves $|Z'|$ F_1 particles combining with one F_2 particle to form a $U(1)'$-neutral dark state, which will be called D^0 (recall Z' is the charge ratio of F_2 and F_1). We would like to know when (at what temperature or, equivalently, redshift) does dark recombination happen, that is, the moment in which the *last* F_1 recombines with the state formed by $|Z'|$-1 F_1 particles and one F_2. Let us call this last state D^+ (we take the convention where F_1 has charge -1 and F_2 has charge $|Z'|$). The relevant process to look at is

$$F_1 + D^+ \leftrightarrow D^0 + \gamma_D. \qquad (32)$$

The Saha equation for the process above is given in e.g. [3]

$$\frac{n_{D^0}}{n_{D^+} n_{F_1}} = \frac{n_{D^0}{}^{(0)}}{n_{D^+}{}^{(0)} n_{F_1}{}^{(0)}}, \qquad (33)$$

where the superscript $^{(0)}$ denotes the equilibrium value. Note that in writing Eq. (33) it has been assumed that $n_{\gamma_D} = n_{\gamma_D}{}^{(0)}$. It is worth stressing that Eq. (33) is an approximate equilibrium equation, namely, the equilibrium limit of the Boltzmann equations. It does not, therefore, follow the

abundances through out-of-equilibrium processes, such as freeze-out (see for instance [3]). Equation (33), nonetheless, predicts the correct redshift of dark recombination, which is the quantity we wish to determine.

To proceed, it is useful to introduce the ionization fraction of F_1,

$$\chi \equiv \frac{n_{F_1}}{n_{F_2}} = \frac{n_{F_1}}{n_{F_1} + n_{D^0}} = \frac{n_{F_1}}{n_{D^+} + n_{D^0}}, \qquad (34)$$

where n_{F_1} is the number density of free F_1 particles and n_{F_2} is the total number density of F_2. The last equality follows from assuming $U(1)'$ neutrality. The left-hand side of Eq. (33) is then $(1 - \chi)/(n_{F_2}\chi^2)$. The right-hand side of Eq. (33) can also be expressed in a more useful form. For a species A of mass m_A and temperature T_A, the equilibrium number density in the limit $m_A \gg T_A$ can be written as (see e.g. [3])

$$n_A = g_A \left(\frac{m_A T_A}{2\pi} \right)^{\frac{3}{2}} e^{-\frac{m_A - \mu_A}{T_A}}, \qquad (35)$$

with μ_A being the chemical potential of the species and g_A a degeneracy factor that usually takes into account multiple spin states. To good approximation $\mu_{\gamma_D} = 0$ so, as long as the equilibrium holds, the following is true:

$$\mu_{F_1} + \mu_{D^+} = \mu_{D^0}. \qquad (36)$$

The ionization energy of D^0, I', is defined to be

$$I' = m_{F_1} + m_{D^+} - m_{D^0}. \qquad (37)$$

Equation (33) can be rearranged in a form which is more useful for following the evolution of the ionization fraction of F_1. To do so, we can employ the fact that $g_{F_1} g_{D^+} = g_{D^0}$ and work in the approximation $m_{D^+} \simeq m_{D^0} \simeq m_{F_2}$. This approximation is valid as long as $m_{F_2} \gg m_{F_1}$ which is assumed.[9] These considerations allow the right-hand side of Eq. (33) to be rearranged to the form

$$\frac{n_{D^0}{}^{(0)}}{n_{D^+}{}^{(0)} n_{F_1}{}^{(0)}} = \left(\frac{2\pi}{m_{F_1} T_{\gamma_D}} \right)^{\frac{3}{2}} e^{\frac{I'}{T_{\gamma_D}}}. \qquad (38)$$

The end result is that the Saha equation [Eq. (33)] can be reduced to the more suitable form

$$\frac{1 - \chi}{\chi^2} = n_{F_2} \left(\frac{2\pi}{m_{F_1} T_{\gamma_D}} \right)^{\frac{3}{2}} e^{\frac{I'}{T_{\gamma_D}}}. \qquad (39)$$

The F_2 number density simply scales with the baryon number density as follows:

---

[9]This approximation is similar to that of approximating the mass of the hydrogen atom with the proton mass.

$$n_{F_2} = \left(\frac{\Omega_{\text{dm}}}{\Omega_{\text{b}}}\right)\left(\frac{m_p}{m_{F_2}}\right)n_B = \left(\frac{\Omega_{\text{dm}}}{\Omega_{\text{b}}}\right)\left(\frac{m_p}{m_{F_2}}\right)\left(\frac{n_B}{n_\gamma}\right)\left(\frac{n_\gamma}{n_{\gamma_D}}\right)n_{\gamma_D},$$
(40)

where $m_p \simeq 0.94$ GeV is the proton mass and $\eta \equiv n_B/n_\gamma$ is the baryon-to-photon ratio. Using $\Omega_{\text{dm}}/\Omega_{\text{b}} \simeq 5.4$ [44], $\eta \simeq 6 \times 10^{-10}$ [51], $n_\gamma/n_{\gamma_D} = (T_\gamma/T_{\gamma_D})^3$ [with T_γ/T_{γ_D} evaluated using Eq. (23)] and $n_{\gamma_D} = \pi^2 T_{\gamma_D}^3/45$ allows us to rewrite Eq. (39) in the following form:

$$\frac{1-\chi}{\chi^2} = A\left(\frac{T_{\gamma_D}}{I'}\right)^{\frac{3}{2}} e^{\frac{I'}{T_{\gamma_D}}},$$
(41)

where

$$A \simeq 3.5 \times 10^{-7} \left(\frac{10^{-9}}{\epsilon}\right)^{\frac{3}{2}}\left(\frac{\mathcal{M}}{m_e}\right)^{\frac{3}{4}}\left(\frac{\text{GeV}}{m_{F_2}}\right)\left(\frac{I'}{m_{F_1}}\right)^{\frac{3}{2}}.$$
(42)

Using the variable $\xi \equiv I'/T_{\gamma_D}$, Eq. (41) can be put to the form

$$\frac{1-\chi}{\chi^2} = A\xi^{-\frac{3}{2}}e^{\xi}.$$
(43)

The Saha equation can be used to determine the redshift of dark recombination. To solve for the redshift (or, equivalently, temperature) of dark recombination, we take $\chi \approx 0.1$, so that Eq. (43) reduces to

$$\xi = \frac{3}{2}\ln\xi + \ln\left(\frac{90}{A}\right).$$
(44)

In this form the Saha equation is easy to solve numerically. Once the value of ξ that solves the equation has been found, the temperature of the dark sector at dark recombination, T'_{dr}, is given by

$$T'_{\text{dr}} = \frac{I'}{\xi}.$$
(45)

The corresponding temperature of the visible sector at the time of dark recombination, T_{dr}, can be found by inverting Eq. (23),

$$T_{\text{dr}} \simeq 3.2 T'_{\text{dr}}\left(\frac{10^{-9}}{\epsilon}\right)^{\frac{1}{2}}\left(\frac{\mathcal{M}}{m_e}\right)^{\frac{1}{4}}.$$
(46)

B. Binding energy of the dark bound state

To make progress, we need to determine I' in terms of the parameters of our model. The bound system of F_2 with N F_1 particles is completely analogous to that of nuclei with N electrons. It follows that the binding energy of the dark state has the general form,

$$I' = Z'^2_{\text{eff}}\frac{\alpha'^2}{2}\mu_R,$$
(47)

where μ_R is the reduced mass of the F_1-D^+ system, given by $\mu_R = m_{F_1}m_{D^+}/(m_{F_1} + m_{D^+})$. In the limit where $m_{F_2} \gg m_{F_1}$ one has that $I' \simeq Z'^2_{\text{eff}}\alpha'^2 m_{F_1}/2$.

Naturally exact analytic expressions for Z'_{eff} are in general unknown, but it is still possible to make a rough approximation for Z'_{eff} and hence determine I'. The charge Z'_{eff} depends only on the chemistry (or equivalently on quantum mechanics) of the bound state we are analyzing. In particular, it depends on shielding effects due to the $|Z'|$-1 F_1 particles partially shielding the charge of the F_2 particle from the last F_1 which is about to combine. The problem of determining Z'_{eff} is therefore identical to that of determining the shielding of an ordinary nucleus of atomic number $Z = |Z'|$ due to Z-1 electrons. It essentially only depends on the way the fermions arrange themselves in orbitals, which in turn is determined solely by quantum mechanics.

Under these assumptions the binding energy I' of the dark bound state can be derived simply by scaling the binding energy I of the corresponding ordinary element with atomic number $Z = |Z'|$ via

$$I' = \left(\frac{\alpha'}{\alpha}\right)^2\left(\frac{m_{F_1}}{m_e}\right)I.$$
(48)

A plot of the binding energies of the elements of the periodic table as a function of the atomic number Z is shown in Fig. 6. One notes from Fig. 6 that, apart from isolated cases such as He, the binding energies of the various elements reside in a fairly narrow range centered at about 10 eV, within a factor of approximately 2. For $Z \gtrsim 10$, the dependence of I on Z is even weaker. This means that $Z'_{\text{eff}} \approx 1$ in Eq. (47) and $I' \approx \alpha'^2 m_{F_1}/2$.
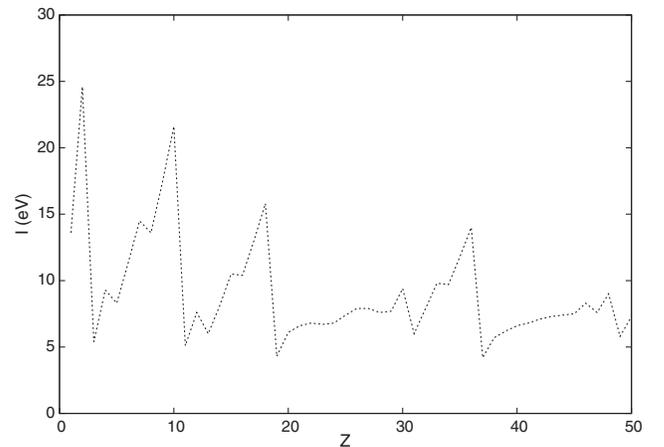

FIG. 6.   Ionization energy as a function of the atomic number for ordinary elements.

C. Exclusion limits

Recall the validity of our model requires $T_{dr} \gtrsim T_{eq}$, where T_{eq} is the temperature of the visible sector at matter-radiation equality. This condition is required for successful LSS formation (e.g. [48]). The redshift of matter-radiation equality is $z_{eq} = 3200 \pm 130$ [51], which leads to a lower limit on the matter-radiation equality temperature of about $T_{eq} = 0.72$ eV.

We can now scan the parameter space of this model and set constraints on its parameters. In principle the model presents five parameters: m_{F_1}, m_{F_2}, α', ϵ and Z'. A numerical analysis of the solution, $T_{dr} \gtrsim T_{eq}$, shows a weak dependence on m_{F_2}. This can be understood by noting that an iterative solution of Eq. (44) displays a loglike dependence on the value of the constant A, which is the only place where m_{F_2} comes into play. The dependence on Z' is also relatively minor, since as previously noted it only affects the binding energy in a modest way.

To summarize, the physics of dark recombination, to a rough approximation, depends on just three parameters: m_{F_1}, α' and ϵ (being relatively insensitive to Z' and m_{F_2}). We now derive constraints on these three parameters.

As already discussed, we derive exclusion limits by requiring $T_{dr} \gtrsim T_{eq}$, and using Eqs. (44), (45), (46), and (48) [we take $I = 10$ eV in Eq. (48)]. In Fig. 7 we give the results for a fixed m_{F_1} and varying α'. The dependence on α', m_{F_1} shown in Fig. 7 can easily be understood by analytical considerations. Recall that to constrain the model we look for the value of parameters for which $T_{dr} \gtrsim T_{eq} \simeq 0.72$ eV. From Eqs. (45) and (48) we have that $T' \propto I' \propto \alpha'^2 m_{F_1}$, while Eq. (23) implies $T_{dr} = T'_{dr} T_{dr}/T'_{dr} \propto \alpha'^2 m_{F_1} \mathcal{M}^{\frac{1}{4}}/\sqrt{\epsilon}$. It follows therefore that the upper limit on ϵ scales as $\alpha'^4 m_{F_1}^2 \sqrt{\mathcal{M}}$. In fact,

the numerical results shown in Fig. 7 give the upper bound on ϵ, coming from dark recombination,

$$\epsilon \lesssim 10^{-8} \left(\frac{\alpha'}{\alpha}\right)^4 \left(\frac{m_{F_1}}{\text{MeV}}\right)^2 \left(\frac{\mathcal{M}}{m_e}\right)^{\frac{1}{2}}. \qquad (49)$$

The above upper bound also includes a factor of ~ 2 uncertainty on ϵ arising from the uncertainty on $I[I = (10 \pm 5)$ eV].

V. GALACTIC STRUCTURE

In this section we explore small-scale phenomenology of this dissipative dark matter model, focusing on the structure of spiral and irregular galaxies at the present epoch. In these galaxies the dark matter halo is (currently) assumed to be in the form of a dissipative plasma composed of F_1 and F_2 particles. Such a plasma can be approximately spherical and extended even in the presence of substantial energy loss due to dissipative processes (such as dark bremsstrahlung) provided there exists a substantial heat source. Spiral and irregular galaxies exhibit ongoing star formation making it possible for ordinary core-collapse supernovae to be this halo heat source (with the halo having evolved as a consequence of the assumed dynamics so that the heating and cooling rates balance). This mechanism requires kinetic mixing with $\epsilon \sim 10^{-9}$ to convert a significant fraction of the supernovae core collapse energy into the production of light F_1, $\bar{F}_1$ particles and ultimately into dark photons. Here, we provide a fairly simplistic analytic treatment of the problem adapting and expanding aspects of previous work in the MDM context [11,12]. This will, of course, only represent a zeroth-order approximation which could be improved in a more sophisticated treatment. Nevertheless, this simple analytic approach provides useful insight and should be adequate for the purposes of extracting the parameter space region of interest.

We will also briefly consider elliptical and dwarf spheroidal galaxies. These galaxies must have a different dark matter structure from spirals and irregulars (at least at the present epoch) as these galaxy types have little current star formation activity. We will briefly comment on how these galaxy types might fit into this picture. The detailed structure of larger systems such as galaxy clusters is of course very important but will be left for future work.

A. Dynamical halo model and halo scaling relations

The physical picture of spiral galaxies is that of a flat disk of baryonic matter surrounded by a dark matter halo. In our model, the dark matter halo is formed by a plasma of F_1 and F_2 particles, where energy is lost to dissipative interactions, such as thermal dark bremsstrahlung. To account for the observed halo structure, a heat source that can replace this energy lost has to exist. In the MDM context, it has been argued that ordinary supernovae can
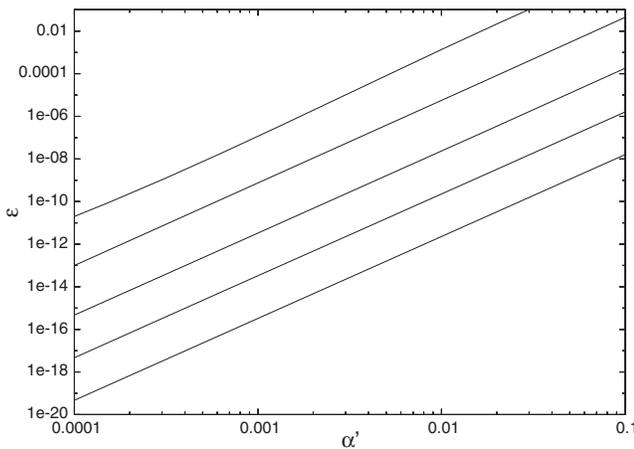

FIG. 7. Exclusion limits from the constraint on the temperature of dark recombination (discussed in text). The limits are for fixed values of m_{F_1} for (going from upper to lower line) $m_{F_1} = 100$, 10, 1, 0.1, 0.01 MeV (excluded region is above the line).

supply this energy [11,12,17]. The mechanism involves kinetic mixing induced processes ($e\bar{e} \to e'\bar{e}'$, $\gamma \to e'\bar{e}'$, ...) in the supernovae core, which can convert $\sim 1/2$ of the core collapse energy into γ', e', $\bar{e}'$ for $\epsilon \sim 10^{-9}$ [25,26] (see also [52]). Ultimately this energy is reprocessed into mirror photons in the region around the supernovae. Essentially the same mechanism can take place in our generic two-component dissipative dark matter model provided that $m_{F_1} \lesssim \text{few} \times T_{SN} \approx 100 \text{ MeV}$.

The physical properties of the dark matter halo are then governed by the Euler equations of fluid dynamics, which take the form

$$\frac{\partial \rho}{\partial t} + \nabla \cdot (\rho \mathbf{v}) = 0,$$

$$\frac{\partial \mathbf{v}}{\partial t} + (\mathbf{v} \cdot \nabla)\mathbf{v} = -\left(\nabla \phi + \frac{\nabla P}{\rho}\right),$$

$$\frac{\partial}{\partial t}\left[\rho(\frac{\mathbf{v}^2}{2} + \mathcal{E})\right] + \nabla \cdot \left[\rho(\frac{\mathbf{v}^2}{2} + \frac{P}{\rho} + \mathcal{E})\mathbf{v}\right] - \rho \mathbf{v} \cdot \nabla \phi$$

$$= \frac{d\Gamma_{\text{heat}}}{dV} - \frac{d\Gamma_{\text{cool}}}{dV}. \tag{50}$$

Here P, ρ and $\mathbf{v}$ denote the pressure, mass density and velocity of the fluid. $\mathcal{E}$ is the internal energy per unit mass of the fluid, so that $\rho(\mathbf{v}^2/2 + \mathcal{E})$ is the energy per unit volume. Finally, Γ_{heat} and Γ_{cool} are the heating and cooling rates. Significant simplifications occur if the system evolves to a static configuration. In this limit, all time derivatives in Eqs. (50) vanish, and if one also assumes spherical symmetry,[10] then Eqs. (50) reduce to just two equations:

$$\frac{d\Gamma_{\text{heat}}(r)}{dV} = \frac{d\Gamma_{\text{cool}}(r)}{dV} \tag{51}$$

and

$$\frac{dP(r)}{dr} = -\rho(r)g(r). \tag{52}$$

Here $g(r) = \nabla \phi$ is the local gravitational acceleration.

The quantities $g(r)$, $P(r)$ can be related to the density $\rho(r)$ via

---

[10]For the most part we assume spherical symmetry. This is a simplifying approximation which we expect will lead to reasonable zeroth order results. Of course, the halo cannot be exactly spherically symmetric; deviations from spherical symmetry might be important and future work could attempt to incorporate these. Two main sources of asymmetry are the supernova heat source, distributed within the galactic disk, and possible bulk rotation of the halo. The latter effect depends on the size of the halos angular momentum, which is unknown and may be difficult to estimate reliably from theoretical considerations.

$$g(r) = \frac{v_{\text{rot}}^2}{r} = \frac{G}{r^2} \int_0^r dr' 4\pi r'^2 \rho_T(r'),$$

$$P(r) = \frac{\rho(r)T(r)}{\bar{m}}, \tag{53}$$

where we have assumed local thermal equilibrium in order to relate P to T and $\bar{m}$ is the mean mass of the particles forming the dark plasma. [$\bar{m} = (n_{F_1}m_{F_1} + n_{F_2}m_{F_2})/(n_{F_1} + n_{F_2})$ for a fully ionized plasma.] Here $\rho_T(r)$ is the total mass density which, in addition to the dark plasma component, $\rho(r)$, includes baryonic components (stars and gas) and possibly compact dark "stars."

A few comments on Eqs. (51) and (52) are in order. Equation (51) represents energy balance at every point in the halo, while Eq. (52) is the hydrostatic equilibrium condition. Both conditions are required for a static configuration. Whether the system is able to evolve to such a static configuration is not certain, but seems possible. Assuming that the system, at an early time prior to the onset of ordinary star formation ($t \lesssim \text{few Gyr}$), was in a more compact configuration, then the subsequent star formation activity would expand and heat the halo (that is, $\Gamma_{\text{heat}} - \Gamma_{\text{cool}} > 0$ initially), which in turn would modify $\Gamma_{\text{heat}} - \Gamma_{\text{cool}}$ via various feedback processes. The idea is that these feedback processes can reduce $\Gamma_{\text{heat}} - \Gamma_{\text{cool}}$ as the halo expands until $\Gamma_{\text{heat}} - \Gamma_{\text{cool}} = 0$ is reached. For example, as the halo expands, the ordinary supernovae rate reduces in response to the weakening gravity, as expressed by the Schmidt-Kennicutt empirical law, which relates the star formation rate to the gas density in spiral galaxies [53],

$$\dot{\Sigma}_\star \propto n_{\text{gas}}^N, \qquad N \sim 1\text{–}2. \tag{54}$$

This mechanism and others can potentially lead to a net reduction in $\Gamma_{\text{heat}} - \Gamma_{\text{cool}}$ as the halo expands, until eventually the static limit is reached where $\Gamma_{\text{heat}} = \Gamma_{\text{cool}}$.

To gain insight, we initially solve Eq. (52) assuming an isothermal halo, i.e. $dT/dr = 0$, and approximating $\rho_T(r) = \rho(r)$. Both of these approximations can be roughly valid in the outer regions of the galaxy. Combining Eqs. (52) and (53) and taking into account the isothermal approximation, the hydrostatic equilibrium equation can be expressed as

$$\frac{d\rho}{dr} = -\frac{\bar{m}\rho(r)G}{Tr^2} \int_0^r dr' 4\pi r'^2 \rho(r'). \tag{55}$$

Equation (55) can be solved by a polynomial of the form $\rho = \lambda/r^p$. Substitution into Eq. (55) yields $p = 2$ and $\lambda = T/2\pi G\bar{m}$, that is,

$$\rho(r) = \frac{T}{2\pi G\bar{m}r^2}. \tag{56}$$

Combining Eqs. (53) and (56) gives us the rotational velocity profile, which we can relate to the temperature of the halo,

$$v_{\rm rot}^2 = \frac{G}{r} \int_0^r dr' 4\pi r'^2 \frac{T}{2\pi G \bar{m} r'^2} = \frac{2T}{\bar{m}}$$

$$\Rightarrow T = \frac{1}{2} \bar{m} v_{\rm rot}^2 \equiv \frac{1}{2} \bar{m} v_\infty^2. \qquad (57)$$

The rotational velocity is found to be independent from the distance to the center of the galaxy, consistent with the observed asymptotically flat rotational curves of spiral galaxies, with asymptotic velocity v_∞.

1. Toy model

Is the assumption of an isothermal halo justified? Let us consider a toy model, where we consider all supernovae as acting as a point source at the Galactic center ($r = 0$) producing a total dark photon luminosity $L_{\rm SN}$. Clearly this model is unphysical and will have to be refined later. To apply Eq. (51) to the system, we have to match the energies absorbed and dissipated within a volume element dV.

Supernovae are presumed to be a source of dark photons, resulting from kinetic mixing induced processes (e.g. $\gamma \to F_1 \bar{F}_1$, $e\bar{e} \to F_1 \bar{F}_1$) occurring in the supernovae cores. The resulting interactions in the region around the supernovae convert this energy into dark photons of an uncertain spectrum. These dark photons can eventually escape and ultimately transport and inject the energy into the halo. Two possible mechanisms can be envisaged: dark photoionization and dark Thomson scattering. We show in Appendix B that dark Thomson scattering is an unimportant heating mechanism for the parameter space we are focusing on ($m_{F_1} \gtrsim 0.1$ MeV).

Assuming, then, that the heating of the halo takes place via a dark photoionization process with cross section $\sigma_{\rm DP}$, the energy per unit time being absorbed in a given volume element, dV, is given by[11]

$$d\Gamma_{\rm heat} = \frac{L_{\rm SN} e^{-\tau}}{4\pi r^2} \sigma_{\rm DP} n_{F_2} dV, \qquad (58)$$

where τ is the optical depth. We have assumed that the two K-shell atomic F_1 states are occupied, which means that the plasma cannot be completely ionized. We shall here assume that the remaining $(|Z'| - 2)$ F_1 states are free, and we will comment more on these consistency conditions in Sec. V B 2. Evidently, the validity of our model then requires $|Z'| \geq 3$.

---

[11]In principle one has to integrate over the frequency spectrum of dark photons, as in [12], but this detail is not essential for the current discussion.

Energy is lost via dark bremsstrahlung of F_1 off F_2. The energy dissipated per unit time within a volume element dV is given by

$$d\Gamma_{\rm cool} = \Lambda(T) n_{F_1} n_{F_2} dV, \qquad (59)$$

where $\Lambda(T)$ is the cooling function for dark bremsstrahlung (defined more precisely in Sec. V B) and n_{F_1} (henceforth) denotes the free F_1 particles number density. There are other sources of dissipation, such as line emission and recombination, which could be included by modifying Λ (see e.g. [54]).[12] Although they might be important, for the purposes of this discussion they will be neglected.[13] Matching of heating and cooling corresponds to equating the right-hand sides of Eqs. (58) and (59), which yields

$$n_{F_1} = \frac{L_{\rm SN} e^{-\tau}}{\Lambda(T) 4\pi r^2} \sigma_{\rm DP}. \qquad (60)$$

If, in addition, we make the assumption that the halo is optically thin ($\tau \ll 1$), we recover $n_{F_1} \propto 1/r^2$. This also means that $\rho \propto 1/r^2$.

The end result is that the assumption of an isothermal halo provides a solution to both energy balance [Eq. (51)] and the hydrostatic equilibrium condition [Eq. (52)]. This suggests that an isothermal halo can be a reasonable approximation at large distances from the Galactic center, where the supernova heat source can be modeled as a point source and where, in addition, $\rho_T(r) \simeq \rho(r)$.

2. A refined model: Solution to the core-cusp problem

The toy model described above is unphysical at $r = 0$. To refine it, we smear the supernova energy source over a finite volume, on a distance scale r_D. Since we are dealing with ordinary supernovae, it is reasonable to assume they are distributed similarly to the mass of the galactic disk. One therefore expects the $\rho \propto 1/r^2$ solution to hold only for $r \gg r_D$. The mass distribution of the galactic disk can be approximated by a profile known as the Freeman disk, with surface density [55]

---

[12]One could also consider inverse Compton scattering, $F_1 \gamma_D \to F_1 \gamma_D$, where γ_D is a dark microwave background photon. For the range of parameter space and physical conditions we are examining, we find that inverse Compton scattering can be neglected except possibly at an early epoch, $z \gtrsim 3$.

[13]A more comprehensive discussion of cooling would have to take into account the cooling efficiency. In general not all bremsstrahlung dark photons will have a mean free path sufficiently long as to escape the halo. Whether they can escape (and hence cool) the halo depends on their location of production and their wavelength. These effects could be incorporated by means of a cooling efficiency function which depends on these variables. However, such a discussion is beyond the scope of our paper and will be left for future work.

$$\Sigma(\tilde{r}) = \frac{m_D}{2\pi r_D^2} e^{-\frac{\tilde{r}}{r_D}}, \qquad (61)$$

with r_D being the disk scale length and m_D its total mass.

We can now follow the same steps as in [17]. Using cylindrical coordinates $(\tilde{r}, \tilde{\theta}, \tilde{z})$ and setting the disk at $\tilde{z} = 0$, the flux at a point $P = (r_1, 0, z_1)$ within an optically thin halo is given by

$$f(r, \cos\phi) = \frac{L_{SN}}{4\pi m_D} \int d\tilde{\theta} \int d\tilde{r}\, \tilde{r} \frac{\Sigma(\tilde{r})}{\tilde{r}^2 - 2\tilde{r}r_1 \cos\tilde{\theta} + r_1^2 + z_1^2}, \qquad (62)$$

where $r = \sqrt{r_1^2 + z_1^2}$ and $\cos\phi \equiv r_1/r$. It is not hard to show that

$$f(r, \cos\phi) \propto \begin{cases} \log r, & r \lesssim r_D, \\ \frac{1}{r^2}, & r \gg r_D. \end{cases} \qquad (63)$$

The energy lost per unit time due to thermal dark bremsstrahlung is once again given by Eq. (59), while the energy absorbed per unit time within a volume element dV now takes the form

$$d\Gamma_{\text{heat}} = f(r, \cos\phi)\sigma_{DP}n_{F_2}dV. \qquad (64)$$

Again equating $d\Gamma_{\text{heat}} = d\Gamma_{\text{cool}}$, using Eqs. (59) and (64), implies $n_{F_1} = f(r, \cos\phi)\sigma_{DP}/\Lambda(T)$. That is, $\rho \propto f(r, \cos\phi)$.

The above considerations regarding the behavior of $f(r, \cos\phi)$ [Eq. (63)] then suggest that $\rho(r)$ can be approximated by a quasi-isothermal dark matter profile,

$$\rho(r) \simeq \frac{\rho_0 r_0^2}{r^2 + r_0^2}, \qquad (65)$$

where $r_0 \sim r_D$, since the latter is the only length scale present in the problem. In Fig. 8 we compare the radial dependence of the solution $\rho \propto f(r, \cos\phi)$ with the quasi-isothermal profile given by Eq. (65), finding good agreement up to $r \simeq r_D$. (Differences at low radii, $r \lesssim r_D$, are not so important as baryons typically dominate the matter density in this region.)

Note that the dark matter density profile obtained in Eq. (65) is cored rather than cuspy (as it would be if $\rho \propto 1/r^2$), with the cored profile arising from having smeared the supernova energy source over a finite volume. This suggests a simple explanation for the inferred existence of dark matter cores in disk galaxies. The inability to explain the cored dark matter profile is one of the shortcomings of collisionless CDM and is referred to as the core-cusp problem (for a review see e.g. [56]). In addition, the scaling relation $r_0 \sim r_D$ is actually implied by measurements of high resolution rotation curves [57],
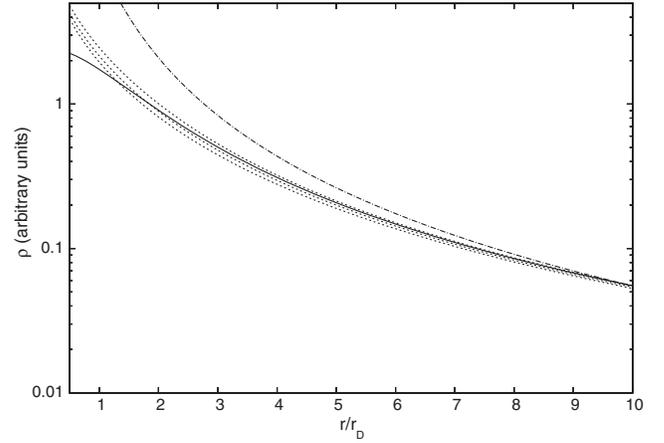

FIG. 8. Comparison between the radial dependence of $\rho \propto f(r, \cos\phi)$, the quasi-isothermal profile given by Eq. (65), and a cuspy profile $\rho \propto 1/r^2$ (in arbitrary units). The dotted lines correspond to $f(r, \cos\phi)$ for (going from the upper to the lower line) $\phi = \pi/4, \pi/3, \pi/2$. The solid line corresponds to a cored density profile (with $r_0/r_D = 1.4$), while the dot-dashed line corresponds to the cuspy profile.

$$\log r_0 = (1.05 \pm 0.11)\log r_D + (0.33 \pm 0.04). \qquad (66)$$

Equation (65) and the scaling relation $r_0 \sim r_D$ have been derived by considering the energy balance within a given galaxy. There is another piece of information we have yet to utilize. That is, demanding that the total energy input must match the total energy output for every disk galaxy.

3. Tully-Fisher relation

If the system evolves to a static configuration, where the heating and cooling rates balance, then the properties of galactic halos will be constrained. Moreover, since heating is proportional to the supernovae rate and cooling is related to the properties of dark matter, energy balance will imply a connection between the baryonic and dark matter components in spiral galaxies. The heating rate of the halo in a given spiral galaxy can be expressed as

$$\Gamma_{\text{heat}} = f_{SN}\langle E_{SN}\rangle R_{SN}, \qquad (67)$$

where E_{SN} is the total energy output from each supernova, and R_{SN} is the rate at which supernovae occur. The fraction of energy which is absorbed by the halo, f_{SN}, is given by

$$f_{SN} = R_{\gamma_D}\langle(1 - e^{-\tau})\rangle, \qquad (68)$$

where the fraction of the total energy output in dark particles is $R_{\gamma_D} \equiv E_D/E_{SN}$, E_D being the amount of energy released from the supernova which is ultimately converted into the creation of dark photons. As a measure of the average optical depth, we consider dark photons propagating from the Galactic center to the edge of the galaxy (approximated as $r \to \infty$),

$$\tau = \int_0^\infty dr \sigma_{\text{DP}} n_{F_2} = \int_0^\infty dr \sigma_{\text{DP}} \rho \kappa = \frac{\pi \sigma_{\text{DP}} \kappa \rho_0 r_0}{2}, \quad (69)$$

where we have made use of the density profile given in Eq. (65) and related the density to the F_2 number density via

$$\rho = n_{F_2}(m_{F_2} + |Z'| m_{F_1}) \equiv \frac{n_{F_2}}{\kappa}. \quad (70)$$

Combining Eqs. (67) and (70) it follows that, in the optically thin limit, the heating rate for the halo of a given spiral galaxy is

$$\Gamma_{\text{heat}} = \frac{\pi R_{\gamma_D} \sigma_{\text{DP}} \kappa \langle E_{\text{SN}} \rangle}{2} \rho_0 r_0 R_{\text{SN}}. \quad (71)$$

The differential cooling rate of the halo is given by Eq. (59). To obtain the total cooling rate Eq. (59) has to be integrated into the volume element. In doing so, note that the differential cooling rate depends on the parameters defining the dark matter density profile, ρ_0 and r_0, through $n_{F_1} \approx \rho \kappa(|Z'| - 2)$ and $n_{F_2} = \rho \kappa$.[14] Integrating Eq. (59) yields

$$\Gamma_{\text{cool}} = \Lambda(T)\kappa^2(|Z'| - 2)\rho_0^2 r_0^4 \int_0^\infty dr' \frac{4\pi r'^2}{(r'^2 + r_0^2)^2}$$
$$= \pi^2 \kappa^2(|Z'| - 2)\Lambda(T)\rho_0^2 r_0^3. \quad (72)$$

Under the assumption that the main source of dissipation is thermal dark bremsstrahlung, $\Lambda(T) \propto \sqrt{T}$ (see e.g. [54]). The temperature T is related to the rotational velocity of the galaxy far from the center, v_∞, via Eq. (57), so that $\Lambda(T) \propto \sqrt{T} \propto v_\infty$. The rotational velocity profile (having neglected baryonic contributions), $v_{\text{rot}}(r)$, can be related to ρ_0 and r_0 via Eq. (53),

$$v_{\text{rot}}^2 = \frac{G}{r} \int_0^r dr' 4\pi r'^2 \frac{\rho_0 r_0^2}{r'^2 + r_0^2}$$
$$= 4\pi G \rho_0 r_0^2 \left[1 - \frac{r_0}{r} \tan^{-1}\left(\frac{r}{r_0}\right) \right]. \quad (73)$$

For $r \gg r_D$, we then have

$$v_\infty = (4\pi G \rho_0 r_0^2)^{\frac{1}{2}}. \quad (74)$$

Imposing the energy balance condition [Eq. (51)], and hence equating $\Gamma_{\text{heat}} = \Gamma_{\text{cool}}$, with Γ_{heat} and Γ_{cool} given by Eqs. (71) and (72), we find

$$\Lambda(T)\rho_0 r_0^2 = \frac{R_{\gamma_D} \sigma_{\text{DP}} \langle E_{\text{SN}} \rangle}{2\pi \kappa(|Z'| - 2)} R_{\text{SN}}. \quad (75)$$

This represents a scaling relation connecting dark matter properties (ρ_0 and r_0) with baryonic properties, such as R_{SN} (and is independent of the previously obtained $r_0 \sim r_D$ relation). We show below that it is roughly equivalent to the empirical Tully-Fisher relation. Combining Eqs. (74) and (75) and recalling that $\Lambda(T) \propto v_\infty \propto (\rho_0 r_0^2)^{\frac{1}{2}}$ results in a scaling relation connecting the supernovae rate and the asymptotic rotational velocity in a given spiral galaxy,

$$R_{\text{SN}} \propto v_\infty^3. \quad (76)$$

Supernovae observational studies have found the relation $R_{\text{SN}} \propto (L_B)^{0.73}$ [58], where L_B is the galaxy B-band luminosity. Combining this relation with that in Eq. (76) yields

$$L_B \propto v_\infty^4. \quad (77)$$

Equation (77) is one of the forms of the Tully-Fisher relation (see e.g. [59]), an empirical relation that is observed to hold for spiral galaxies [60] and used extensively as a rung on the cosmic distance ladder (see for instance [61]). The general form of the Tully-Fisher relation is $L \propto (v_{\text{rot}})^\alpha$, where the power α depends on the luminosity band under consideration. For instance, for the K band (near infrared) $\alpha = 4.35 \pm 0.14$ is determined [59], while for the optical B band $\alpha = 3.91 \pm 0.13$ is found [59]. The Tully-Fisher relation is currently unexplained, although it suggests a deep connection between the baryonic and dark matter components of spiral galaxies. Our model seems to supply such a connection via the nontrivial dissipative dynamics: the Tully-Fisher relation is the energy balance condition, Eq. (51), where Γ_{heat} arises from supernovae heating and Γ_{cool} from dissipative dynamics.[15] This scenario is expected to hold within irregular galaxies as well, since these galaxies have ongoing star formation–like spirals.

4. Elliptical galaxies: The Faber-Jackson relation

The dynamical halo model, with heating powered by kinetic mixing induced processes in the core of ordinary supernovae balancing the energy loss due to dissipative processes in the halo, seems to be viable for galaxies with ongoing star formation: that is, spiral and irregular galaxies. This picture cannot be directly applied to elliptical galaxies or dwarf spheroidal galaxies as these galaxies are devoid of

---

[14]The relation $n_{F_1} \approx \rho \kappa(|Z'| - 2)$ assumes the plasma is not fully ionized, but has the K-shell states occupied, so that dark photoionization can occur. More generally, $n_{F_1} = f \rho \kappa(|Z'| - 2)$, where $f \leq 1$ accounts for partial ionization of the remaining atomic states.

[15]It is worth mentioning that a third relation, not independent from the other two ($r_0 \propto r_D$ and $L_B \propto v_\infty^4 \propto \rho_0^2 r_0^4$), can be obtained. Observational studies have shown that $m_D \propto (L_B)^{1.3}$ [62] and $r_D \propto (m_D)^{0.38}$ [63]. Combining these relations yields $\rho_0 r_0 \approx$ const (which is observed to hold in spiral galaxies [64,65]).

baryonic gas and exhibit suppressed star formation. Focusing first on ellipticals (we briefly discuss dwarf spheroidals in the following subsection) it is possible that these galaxies could have evolved from spirals. In particular, spirals may have a final evolutionary stage where they have exhausted their baryonic gas to the point where the ordinary supernova rate is insufficient to support the dark halo from collapse.

Consider the limiting case where $t_{\rm cool} \ll t_{\rm ff}$, with $t_{\rm cool}$ and $t_{\rm ff}$ being the cooling and free-fall time scales, respectively. In this limit, the dark halo can cool and potentially fragment into dark stars. Imagine a point in time where the heating suddenly stops and the halo cools but does not have time yet to collapse (consistently with $t_{\rm cool} \ll t_{\rm ff}$). The total energy at this time can be approximated as just the gravitational potential energy and is given by

$$U_i = - \int_0^R dr 4\pi r^2 \frac{GM_r}{r} \rho(r),$$ (78)

where the mass enclosed within a radius r is

$$M_r = \int_0^r dr' 4\pi r'^2 \rho(r') \simeq 4\pi \rho_0 r_0^2 r.$$ (79)

In evaluating M_r above, we have used the density profile given by Eq. (65). In the limit where $t_{\rm cool} \ll t_{\rm ff}$, this should be a good approximation, as the dark matter density profile has no "time" to change. Evaluating the integral in Eq. (78) then gives

$$U_i = -4\pi \rho_0 r_0^2 GM_t,$$ (80)

where the total mass is $M_t = \int_0^R dr 4\pi r^2 \rho \simeq 4\pi \rho_0 r_0^2 R$.

As the system contracts, and assuming dark stars form, these stars would attain kinetic energy as they fall into the gravitational potential well. The virial theorem can then be used to relate their eventual kinetic energy, in terms of the eventual potential energy: $U_f = -2T_f$. Thus, equating this final energy with the initial energy gives

$$U_i = U_f + T_f = -T_f.$$ (81)

By using $T_f = 3M_t \sigma_v^2/2$, where σ_v is the average velocity dispersion of the dark stars, we find that

$$\sigma_v^2 = \frac{8\pi G \rho_0 r_0^2}{3}.$$ (82)

If, in addition, we make the assumption that the ordinary stars "thermalize" with the dark stars, it follows that their velocity dispersion will also be approximately σ_v^2. Given that the elliptical galaxy in the picture evolved from a spiral galaxy, the ρ_0, r_0 parameters obey the scaling relations derived earlier. Using the scaling relation $\rho_0 r_0 \approx$ const and $r_0 \propto r_D \propto \sqrt{L_B}$, which follows from $m_D \propto (L_B)^{1.3}$ [62]

and $r_D \propto (m_D)^{0.38}$ [63], we obtain a relation between the B-band luminosity of a given elliptical galaxy and its velocity dispersion,

$$L_B \propto \sigma_v^4.$$ (83)

Such a scaling relation, known as the Faber-Jackson relation [66], is observed to roughly hold for elliptical galaxies.

This picture of elliptical galaxies might help explain some of their distinctive properties. In particular, if the dark stars produce dark supernovae, then kinetic mixing induced processes in the core of these dark supernovae can generate a large flux of ionizing ordinary photons, which can heat ordinary matter, thereby potentially explaining why elliptical galaxies are observed to be devoid of baryonic gas.

5. Dwarf spheroidal galaxies

Dwarf spheroidal galaxies, like ellipticals, are also devoid of baryonic gas and show little star formation activity (at the present epoch). It is possible that they reach this point in their evolution in a manner broadly analogous to the picture just described above for ellipticals (although their formation may have been very different). That is, at an earlier stage in their evolution these galaxies had a dark matter plasma halo which had dynamically evolved into a steady state configuration featuring hydrostatic equilibrium and with heating and cooling rates balanced. Then at some point, perhaps due to insufficient star formation to keep up with the heating requirements, the halo collapsed and fragmented into dark stars. If this dark star formation rate is rapid enough, the dark matter structural properties of the galaxy can be preserved. In this manner it might be possible to explain why dwarf spheroidal galaxies, irregular and spiral, and ellipticals all have broadly similar dark matter structural properties as indicated from observations (e.g. the inferred dark matter surface density, $\rho_0 r_0$, is roughly constant independent of galaxy type [65]).

Although the middle and latest stages in the evolution of dwarf spheroidal and elliptical galaxies might be similar (as discussed above), their formation may have been very different. Studies of the dwarf spheroidal population around the Andromeda (M31) galaxy show that a large fraction of these satellites orbit in a thin plane [67]. (A similar planar structure of satellites, although not quite so impressive, has also been observed around the Milky Way [68].) These observations can potentially be explained if the dwarf spheroidal galaxies formed during a major merger event, so that they are in fact tidal dwarf galaxies [69]. Even if a significant fraction of dwarf spheroidal galaxies formed in this way, they can still be dark matter dominated and have evolved via the dissipative dynamics so that their current structural properties are consistent with observations (e.g. with scaling relations

such as the roughly constant dark matter surface density, $\rho_0 r_0$). At the earliest stages of galaxy formation, prior to ordinary star formation, the dark matter which seeded the galaxy may have collapsed into a disk due to the dissipative processes. Subsequently the ordinary baryons also formed a disk. Gravitational interactions between the two disks can cause them to merge on a fairly short time scale, cf. [24]. A major galaxy merger event around this time could have produced tidal dwarf galaxies with a large dark matter fraction (as the dark matter particles in the disk have velocities correlated with the baryonic particles). The observed alignment of the satellite galaxies around M31 can thereby be potentially explained, as was discussed for the mirror dark matter case [70]. Of course, the formation of the ordinary disk and consequent ordinary star generation and supernovae will lead to the production of dark photons (via kinetic mixing induced processes). This energy is presumed to eventually heat and expand the disk dark gas component of the host galaxy (in this case M31) into its current state: a roughly spherical halo.

B. Consistency conditions and energy balance

The assumption that the system evolves to a static configuration has allowed us to establish a connection between the baryonic and dark matter components in disk galaxies, in the form of scaling relations which are consistent with observations. We now wish to understand how this energy balance argument can constrain the five-dimensional parameter space of our dark matter model. This requires a more quantitative understanding of the exact heating and cooling mechanisms.

As previously discussed, thermal dark bremsstrahlung of F_1 off F_2 is assumed to be the dominant dissipation avenue. The energy lost per unit time per unit volume due to this process is given in e.g. [54]

$$\frac{d\Gamma_{\text{cool}}}{dV} = \frac{16\alpha'^3 (2\pi T)^{\frac{1}{2}}}{(3m_{F_1})^{\frac{3}{2}}} Z'^2 n_{F_1} n_{F_2} \bar{g}_B, \qquad (84)$$

where $\bar{g}_B \simeq 1.2$ is the frequency average of the velocity-averaged Gaunt factor for thermal bremsstrahlung.

The temperature, T, in Eq. (84), is related to the mean mass of the dark plasma. In the limit where $m_{F_2} \gg m_{F_1}$, and assuming the two K-shell atomic states are occupied, neutrality of the plasma implies that the number density of free F_1 states is $n_{F_1} = (|Z'| - 2)n_{F_2}$. In this circumstance the mean mass can be approximated by

$$\bar{m} = \frac{n_{F_1} m_{F_1} + n_{F_2} m_{F_2}}{n_{F_1} + n_{F_2}} \approx \frac{m_{F_2}}{|Z'| - 1}. \qquad (85)$$

Using Eqs. (57), (65), (70), (74), (84), and (85), the total cooling rate can be expressed as

$$\Gamma_{\text{cool}} = 32\pi^3 \bar{g}_B \alpha'^3 Z'^2 (|Z'| - 2)\kappa^2 \sqrt{\frac{Gm_{F_2}}{27(|Z'| - 1)m_{F_1}^3}} (\rho_0 r_0)^{\frac{5}{2}} r_0^{\frac{3}{2}}. \qquad (86)$$

In the MDM framework it has been argued that photoionization of K-shell mirror electrons in a mirror metal component can replace the energy lost due to dissipation. This process can take place because the mirror metals in question retain their K-shell mirror electrons [17]. If we assume that in our model D^0 (the dark bound state), albeit being close to fully ionized, retains its K-shell F_1 particles, then a similar mechanism, which we call *dark photoionization*, can efficiently heat the halo. The cross section for dark photoionization, σ_{DP}, can easily be obtained from that of ordinary photoionization, found in e.g. [54]

$$\sigma_{\text{DP}} = \frac{g' 16\sqrt{2}\pi}{3m_{F_1}^2} \alpha'^6 |Z'|^5 \left(\frac{m_{F_1}}{E_{\gamma_D}}\right)^{\frac{7}{2}}, \qquad (87)$$

where $g' = 1, 2$ counts the number of K-shell F_1 particles present.

For the picture we have just presented to be valid, a series of consistency conditions will have to hold. We will now proceed to discuss what these conditions are and how they constrain the available parameter space for our model.

1. Cooling time scale

The dynamical halo picture, governed by a balance between heating and cooling rates, could only hold provided the cooling time scale is much less than the Hubble time. This requirement constrains the available parameter space and, as one can see from Eq. (86), will set an upper bound on the mass of F_2 [recall $\kappa^{-1} = (m_{F_2} + |Z'|m_{F_1})$]. If n_T is the total number density of dark particles, the cooling time scale is given by

$$t_{\text{cool}} \approx \frac{\frac{3}{2} n_T T}{\Lambda(T) n_{F_1} n_{F_2}} \approx \frac{3T}{2\Lambda(T) n_{F_2}}, \qquad (88)$$

where we have approximated $n_T \approx n_{F_1}$. Making use of Eqs. (57), (70), (84), and (85), we can write

$$t_{\text{cool}} \approx \frac{9\sqrt{3}}{64\bar{g}_B \sqrt{\pi}} \sqrt{\frac{m_{F_2} m_{F_1}^3}{|Z'| - 1}} \frac{v_{\text{rot}}}{\kappa \rho \alpha'^3 Z'^2}. \qquad (89)$$

Observe that the cooling time scale can be defined locally, i.e. $t_{\text{cool}}(r)$, through the dependence on $\rho(r)$. Less dense regions cool more slowly, so the most stringent limit occurs where $\rho(r)$ is lowest. Of course we have little knowledge about halo properties far from the Galactic center. As a rough limit, we shall require $t_{\text{cool}}(r) \lesssim$ few billion years, for $r \lesssim 3.2r_D \sim 2r_0$ (3.2 r_D is the optical radius where most of

the baryons reside, defined in e.g. [71]). Note that the most stringent limits occur for the largest disk galaxies, where $\rho(r = 2r_0) \approx \rho_0/5$ and $v_{\rm rot} \approx 300$ km/s. Here we have taken the typical values (for large disk galaxies) $\rho_0 r_0 \simeq 100$ M$_\odot$/pc^2 and $r_0 \simeq 20$kpc and hence $\rho_0/5 \simeq 10^{-3}$ M$_\odot$/pc^3. In this case, the requirement $t_{\rm cool}(r = 2r_0) \lesssim$ few billion years gives the upper limit on the mass of F_2,

$$m_{F_2} \lesssim 200 \left(\frac{\rm MeV}{m_{F_1}}\right) \left(\frac{\alpha'}{10^{-2}}\right)^2 \left(\frac{|Z'|}{10}\right)^{\frac{5}{3}} {\rm GeV}. \quad (90)$$

2. Ionization state of the halo

The scenario described earlier assumed that the halo is ionized but the dark bound state, D^0, retains its K-shell F_1 particles. The former requirement allows for efficient cooling via dark bremsstrahlung, while the latter is a necessary condition for dark photoionization to take place. Here we require such a picture to hold for all disk galaxies, regardless of size. Were this not the case, one would expect significant observational differences in moving along the spectrum of disk galaxies, depending on whether their dark plasma is ionized or D^0 retains its K-shell F_1 particles. Hence we require the temperature of the halo, given in Eq. (57), to be high enough to ensure that D^0 is ionized (at least one free F_1 particle per bound state), while being low enough to allow the K-shell F_1 particles to be retained.

By comparing the appropriate ionization and capture cross sections, in Appendix A we estimate that, given the ionization energy $\mathcal{I}$, the transition from an ionized to a neutral halo occurs at a temperature $T = \mathcal{I}/\xi$, where $\xi \approx 7 - 28$. Of course, in the process of obtaining a conservative lower bound on the mass of the F_2 particle, we are interested in the maximum value ξ can assume, that is, $\xi_{\rm max} \approx 28$. Similarly, to obtain a conservative upper bound on m_{F_2}, we are interested in the minimum value ξ can assume in relation to the process of K-shell photoionization. In Appendix A we estimate that $\xi_{\rm min} \approx \min[1/(\alpha'^3 Z'^4), 1]$, and hence, denoting by $\mathcal{J}$ the relevant ionization energy, we obtain the rough conditions,

$$T \gtrsim \frac{\mathcal{I}}{\xi_{\rm max}}$$
$$\Rightarrow \frac{m_{F_2}}{\rm GeV} \gtrsim \left(\frac{|Z'|}{10}\right) \left(\frac{\alpha'}{10^{-2}}\right)^2 \left(\frac{m_{F_1}}{\rm MeV}\right) \left(\frac{50 \text{ km/s}}{v_{\rm rot}}\right)^2,$$
$$T \lesssim \frac{\mathcal{J}}{\xi_{\rm min}}$$
$$\Rightarrow \frac{m_{F_2}}{\rm GeV} \lesssim 100 \left(\frac{|Z'|}{10}\right)^3 \left(\frac{\alpha'}{10^{-2}}\right)^2 \left(\frac{m_{F_1}}{\rm MeV}\right) \left(\frac{300 \text{ km/s}}{v_{\rm rot}}\right)^2$$
$$\times g(\alpha', Z'), \quad (91)$$

where $g(\alpha', Z') \equiv \max(\alpha'^3 Z'^4, 1)$. Clearly the most stringent lower bound on m_{F_2} arises from the smallest spiral and irregular galaxies, with $v_{\rm rot} \approx 50$ km/s, while the most stringent upper bound comes from the biggest disk galaxies, for which $v_{\rm rot} \approx 300$ km/s, and thus

$$\left(\frac{|Z'|}{10}\right) \left(\frac{\alpha'}{10^{-2}}\right)^2 \left(\frac{m_{F_1}}{\rm MeV}\right) \lesssim \frac{m_{F_2}}{\rm GeV}$$
$$\lesssim 100 \left(\frac{|Z'|}{10}\right)^3 \left(\frac{\alpha'}{10^{-2}}\right)^2 \left(\frac{m_{F_1}}{\rm MeV}\right)$$
$$\times g(\alpha', Z'). \quad (92)$$

In addition, we have to require that the upper bound on m_{F_2} [Eq. (90)] be greater than the respective lower bound [Eqs. (91)]. Doing so yields

$$|Z'| \gtrsim 4 \left(\frac{m_{F_1}}{10 \text{ MeV}}\right)^3. \quad (93)$$

It is conceivable that the ionization physics sets the physical scale of spiral and irregular galaxies (i.e. sets either or both $v_{\rm rot}^{\rm max}$, $v_{\rm rot}^{\rm min}$), which means that either or both the limits in Eq. (92) are equalities. Equating the two bounds in Eq. (92) we obtain that this limiting situation occurs for $|Z'| \sim 1$.

3. Energy balance

We now turn to the energy balance condition, $\Gamma_{\rm heat} = \Gamma_{\rm cool}$ [Eq. (51)]. As previously discussed, we have assumed that the galactic system evolves such that this condition is currently satisfied for disk galaxies. Given the observed properties of disk galaxies, we can use this condition to constrain the fundamental parameters of our model.

The cooling rate, assuming the main dissipation process being dark bremsstrahlung, is readily found [Eq. (86)]. For the heating rate the situation is more complicated. Details about $\Gamma_{\rm heat}$ require a detailed understanding of the frequency spectrum of the dark photons which, it is alleged, heat the halo. Nevertheless, we can set an upper limit on the value of this heating rate,

$$\Gamma_{\rm heat} \lesssim R_{\gamma_D} R_{\rm SN} \langle E_{\rm SN} \rangle \min(\tau_{\rm max}, 1), \quad (94)$$

where $\tau_{\rm max}$ is the maximum value the optical depth [Eq. (69)] can take after allowing for all possible forms of the γ_D spectrum. Equations (69) and (87) suggest that the optical depth is maximized when $E_{\gamma_D} = I'$, where $I' \approx Z'^2 \alpha'^2 m_{F_1}/2$ is the ionization energy of the relevant K-shell F_1 particle; hence

$$\tau_{\max} = \frac{256\pi^2}{3} \frac{\rho_0 r_0}{m_{F_1}^2 m_{F_2} \alpha' Z'^2}. \tag{95}$$

Assuming the nominal value $\rho_0 r_0 \approx 100 \ M_\odot/\mathrm{pc}^2 \simeq 4.6 \times 10^{-6} \ \mathrm{GeV}^3$ and taking the upper bound on m_{F_2} given in Eq. (92), we get

$$\tau_{\max} \gtrsim 40 \left(\frac{\mathrm{MeV}}{m_{F_1}}\right)^3 \left(\frac{10^{-2}}{\alpha'}\right)^3 \left(\frac{10}{|Z'|}\right)^5 \frac{1}{g(\alpha', Z')}. \tag{96}$$

Equation (96) suggests $\tau_{\max} \gtrsim 1$ holds for a significant fraction of parameter space.

Let us now assume parameters where $\tau_{\max} \gtrsim 1$ and evaluate an upper limit for Γ_{heat} [note that even with parameters where $\tau_{\max} \lesssim 1$, the derived limit will still be valid, given that $\min(\tau_{\max}, 1) \leq 1$]. For $\epsilon \lesssim 10^{-9}$, $R_{\gamma_D} \propto \epsilon^2$, while for $\epsilon \gtrsim 10^{-9}$, R_{γ_D} actually saturates at $\sim 1/2$. By inserting numbers into Eq. (94), we get

$$\Gamma_{\mathrm{heat}} \lesssim \left(\frac{\epsilon}{10^{-9}}\right)^2 \left(\frac{\langle E_{\mathrm{SN}} \rangle}{3 \times 10^{53} \ \mathrm{erg}}\right) \left(\frac{R_{\mathrm{SN}}}{0.03 \ \mathrm{yr}^{-1}}\right) 10^{44} \ \frac{\mathrm{erg}}{\mathrm{s}}, \tag{97}$$

which holds for $\epsilon \lesssim 10^{-9}$. Similarly, inserting numbers into Eq. (86), we obtain the cooling rate for a given galaxy,

$$\Gamma_{\mathrm{cool}} \simeq \left(\frac{\alpha'}{10^{-2}}\right)^3 \left(\frac{\mathrm{MeV}}{m_{F_1}}\right)^{\frac{3}{2}} \left(\frac{|Z'|}{10}\right)^{\frac{5}{2}} \left(\frac{10 \ \mathrm{GeV}}{m_{F_2}}\right)^{\frac{3}{2}}$$
$$\times \left(\frac{\rho_0 r_0}{100 \ \frac{M_\odot}{\mathrm{pc}^2}}\right)^{\frac{5}{2}} \left(\frac{r_0}{5 \ \mathrm{kpc}}\right)^{\frac{3}{2}} 10^{44} \ \frac{\mathrm{erg}}{\mathrm{s}}. \tag{98}$$

The comparison of Eqs. (97) and (98) requires the following approximate relation holds:

$$\mathcal{C}\left(\frac{10^{-9}}{\epsilon}\right)^2 \left(\frac{\alpha'}{10^{-2}}\right)^3 \left(\frac{\mathrm{MeV}}{m_{F_1}}\right)^{\frac{3}{2}} \left(\frac{|Z'|}{10}\right)^{\frac{5}{2}} \left(\frac{10 \ \mathrm{GeV}}{m_{F_2}}\right)^{\frac{3}{2}} \lesssim 1, \tag{99}$$

where

$$\mathcal{C} \equiv \left(\frac{\rho_0 r_0}{100 \ \frac{M_\odot}{\mathrm{pc}^2}}\right)^{\frac{5}{2}} \left(\frac{r_0}{5 \ \mathrm{kpc}}\right)^{\frac{3}{2}} \left(\frac{3 \times 10^{53} \ \mathrm{erg}}{\langle E_{\mathrm{SN}} \rangle}\right) \left(\frac{0.03 \ \mathrm{yr}^{-1}}{R_{\mathrm{SN}}}\right). \tag{100}$$

We expect $\mathcal{C} \approx 1$ to hold for all spirals on account of scaling relations. In addition, Eqs. (90) and (99) provide us with a rough lower bound on ϵ,

$$\epsilon \gtrsim 10^{-10}. \tag{101}$$

Note that this lower bound is consistent with the upper bounds on ϵ derived previously from early universe cosmology.

VI. SUMMARY OF THE BOUNDS ON THE MODEL

Having studied the early universe cosmology and galactic structure implications of the model, we can now make use of our analyses to constrain the five-dimensional parameter space in question. We start by looking at the kinetic mixing parameter, ϵ. The validity of our picture of galaxy structure requires core-collapse supernovae to produce a considerable energy output in light dark particles (specifically, $F_1 \bar{F}_1$ pairs initially) via kinetic mixing induced processes. We have found that $\epsilon \gtrsim 10^{-10}$ is required for the energy output to successfully heat the halo [Eq. (101)]. An upper bound on ϵ was derived in Sec. III from $\delta N_{\mathrm{eff}}[\mathrm{CMB}]$ and $\delta N_{\mathrm{eff}}[\mathrm{BBN}]$ constraints (Fig. 5), which indicate $\epsilon \lesssim 5 \times 10^{-8}$.

As discussed in Sec. II, m_{F_1} is required to be bounded above by about 100 MeV; otherwise $F_1 \bar{F}_1$ pair production becomes exponentially (Boltzmann) suppressed in the core of core-collapse supernovae, where the maximum temperature which can be reached is about 30 MeV. A lower limit of around $m_{F_1} \gtrsim 0.01$ MeV arises from white dwarf cooling and red giants helium flash considerations [26].

A constraint on the dark recombination temperature (so that dark acoustic oscillations do not modify the early growth of LSS) also provided a useful constraint on parameters. This constraint, Eq. (49), together with the above limits on m_{F_1}, ϵ, suggest a lower bound: $\alpha' \gtrsim 10^{-4}$. Further, our analyses implicitly assumed that perturbation theory could reliably be used to calculate cross sections, ionization energies, and so forth, which is valid only if α' is sufficiently small: $\alpha' \lesssim 10^{-1}$.

Constraints on m_{F_2} were derived from galactic structure considerations in Sec. V. There it was shown that a successful picture of spiral and irregular galaxies could be achieved within this two-component hidden sector model provided m_{F_2} satisfies the constraints given by Eqs. (90), (92), and (99).

Below, we summarize the bounds obtained in this work:

$$
\begin{cases}
\epsilon \lesssim \min\left[3.5\times10^{-9}\left(\frac{\mathcal{M}}{m_e}\right)^{\frac{1}{2}}, 10^{-8}\left(\frac{\alpha'}{\alpha}\right)^4\left(\frac{m_{F_1}}{\text{MeV}}\right)^2\left(\frac{\mathcal{M}}{m_e}\right)^{\frac{1}{2}}\right], \\[2mm]
\epsilon \gtrsim 10^{-10}, \\[2mm]
0.01 \text{ MeV} \lesssim m_{F_1} \lesssim 100 \text{ MeV}, \\[2mm]
m_{F_2} \gtrsim \left(\frac{|Z'|}{10}\right)\left(\frac{\alpha'}{10^{-2}}\right)^2\left(\frac{m_{F_1}}{\text{MeV}}\right) \text{ GeV}, \\[2mm]
m_{F_2} \lesssim \min\left[200\left(\frac{\text{MeV}}{m_{F_1}}\right)\left(\frac{\alpha'}{10^{-2}}\right)^2\left(\frac{|Z'|}{10}\right)^{\frac{5}{3}}, 100\left(\frac{|Z'|}{10}\right)^3\left(\frac{\alpha'}{10^{-2}}\right)^2\left(\frac{m_{F_1}}{\text{MeV}}\right)g(\alpha', Z')\right] \text{ GeV}, \\[2mm]
10^{-4} \lesssim \alpha' \lesssim 10^{-1}, \\[2mm]
|Z'| \gtrsim \max\left[3, 4\left(\frac{m_{F_1}}{10\text{MeV}}\right)^3\right],
\end{cases} \tag{102}
$$

where $\mathcal{M} \equiv \max(m_e, m_{F_1})$ and $g(\alpha', Z') \equiv \max(\alpha'^3 Z'^4, 1)$ ($m_e = 0.511$ MeV is the electron mass).

There is a finite, but certainly restricted, region of parameter space consistent with all of the above constraints. For example, if we fix $m_{F_1} = 1$ MeV, $\alpha' = 10^{-2}$, $|Z'| = 10$, the above constraints are all satisfied for $10^{-10} \lesssim \epsilon \lesssim 5 \times 10^{-9}$ and 1 GeV $\lesssim m_{F_2} \lesssim 100$ GeV.

VII. CONCLUDING REMARKS

Dark matter can be accommodated without modifying known Standard Model physics by hypothesizing the existence of a hidden sector. That is, an additional sector containing particles and forces which interact with the known Standard Model particle content predominantly via gravity. We have considered a hidden sector containing two stable particles, F_1 and F_2, charged under an unbroken $U(1)'$ gauge symmetry, hence featuring dissipative interactions. The associated massless gauge field, the dark photon, can interact via kinetic mixing with the ordinary photon. Our analysis indicates that such an interaction, of strength $\epsilon \sim 10^{-9}$, is required in order to explain galactic structure. We calculated the effect of this new physics on BBN and its contribution to the relativistic energy density at hydrogen recombination. Subsequently we examined the process of dark recombination, during which neutral dark states are formed, which is important for LSS formation.

We then analyzed the phenomenology of our model in the context of galactic structure. Focusing on spiral and irregular galaxies, we modeled their halos (at the current epoch) as a plasma composed of dark matter particles, F_1 and F_2. This plasma has a substantial ongoing energy loss due to dissipative processes such as dark bremsstrahlung. Kinetic mixing induced processes in the core of ordinary supernovae can convert a substantial fraction of the gravitational core-collapse energy into dark sector particles (and eventually into dark photons) that ultimately provide the halo energy which compensates for the dissipative energy lost. We found that such a dynamical picture can reproduce several observed features of spiral and irregular galaxies, including the cored density profile and the Tully-Fisher relation. We also discussed how elliptical and dwarf spheroidal galaxies might fit into this framework which we argued has the potential to explain many of their peculiar features.

The above considerations constrain the five Lagrangian parameters of our model, as summarized in Eqs. (102). Note, in particular, that the kinetic mixing coupling, ϵ, is constrained to lie within the range $10^{-10} \lesssim \epsilon \lesssim 5 \times 10^{-8}$. A correct simultaneous explanation of both early Universe cosmology and galactic structure typically requires one fermion, F_1, to be in the MeV range (or just below) and the other to be heavier, in the GeV (or possibly TeV) range.

The allowed mass range of the two fermions means they can be, at least in principle, detected in direct detection experiments. Two types of interactions are of particular interest in this context: F_1-electron scattering and F_2-nuclei scattering. The self-interacting nature of the F_1 and F_2 particles enhances the capture rate of these particles within the Earth, giving rise to a unique signature: a diurnal modulation in the interaction rate. Such an effect is expected to be particularly evident for experiments located in the Southern Hemisphere, giving rise to suppressions in the interaction rate which could be as large as 100% [72].

Although an explanation of the DAMA annual modulation signal [13] in terms of nuclear recoils appears disfavored given the null results of the other experiments, recent work (in the context of MDM) has shown that it might be possible to explain it in terms of dark matter scattering off electrons if the mass of the dark matter particle is in the MeV range [16]. Within the framework of our two-component model, a similar explanation seems possible; that is, the observed annual modulation signal in the DAMA experiment might be due to F_1-electron scattering.

Hidden sector dark matter models can be quite appealing from a theoretical point of view and, as we have shown, can provide a satisfactory explanation for dark matter

phenomena on both large and small scales. In our study we have constrained the parameter space of a particularly simple two component hidden sector model and have indicated potential ways of testing such a model in the context of direct detection experiments.

APPENDIX A: IONIZATION TRANSITION TEMPERATURE

We estimate the quantity ξ in Sec. V B 2. Recall that ξ is defined in terms of the transition temperature between two states, at the relevant ionization energy I', $T = I'/\xi$. Consider, for instance, the process relevant for D^0 ionization, with cross section σ_I,

$$F_1 + D^0 \rightarrow D^+ + F_1 + F_1, \qquad (A1)$$

which is opposed by the corresponding capture process, with cross section σ_C,

$$F_1 + D^+ \rightarrow D^0 + \gamma_D. \qquad (A2)$$

The number density of D^+ is governed by the following rate equation:

$$\frac{dn_{D^+}}{dt} = n_{F_1} n_{D^0} \langle \sigma_I v_{F_1} \rangle - n_{F_1} n_{D^+} \langle \sigma_C v_{F_1} \rangle. \qquad (A3)$$

It follows that in a steady-state situation $n_{D^+}/n_{D^0} = \langle \sigma_I v_{F_1} \rangle / \langle \sigma_C v_{F_1} \rangle$, and hence we compare the relevant thermally averaged ionization and capture cross sections,

$$\langle \sigma_I v_{F_1} \rangle = \sqrt{\frac{1}{m_{F_1}\pi}} \left(\frac{2}{T}\right)^{\frac{3}{2}} \int_{I'}^{\infty} dE_{F_1} E_{F_1} e^{-\frac{E_{F_1}}{T}} \sigma_I,$$

$$\langle \sigma_C v_{F_1} \rangle = \sqrt{\frac{1}{m_{F_1}\pi}} \left(\frac{2}{T}\right)^{\frac{3}{2}} \int_{0}^{\infty} dE_{F_1} E_{F_1} e^{-\frac{E_{F_1}}{T}} \sigma_C. \qquad (A4)$$

The ionization and capture cross sections are given in [73,74] and are roughly[16]

---

[16]The following expressions assume the F_1 particles are nonrelativistic, that is, $T \lesssim m_{F_1}$. If we demand that the non-relativistic approximation is valid for all spirals ($v_{\rm rot} \lesssim 300$ km/s), then we require $m_{F_2}/m_{F_1} \lesssim 10^6(|Z'| - 1)$.

$$\sigma_I \sim \frac{\alpha'^2}{E_{F_1} I'},$$

$$\sigma_C \sim \frac{\alpha'^5 Z'^4}{E_{F_1}(E_{F_1} + I')}. \qquad (A5)$$

The relevant transition will occur when the quantity $\langle \sigma_I v_{F_1} \rangle / \langle \sigma_C v_{F_1} \rangle$ is of order 1, that is,

$$\frac{\langle \sigma_I v_{F_1} \rangle}{\langle \sigma_C v_{F_1} \rangle} \sim \frac{I' + T}{I'} \frac{e^{-\frac{I'}{T}}}{\alpha'^3 Z'^4} \sim 1, \qquad (A6)$$

and hence when

$$\left(1 + \frac{1}{\xi}\right)e^{-\xi} \sim \alpha'^3 Z'^4, \qquad (A7)$$

where $\xi \equiv I/T$.

For the process of D^0 ionization, we can safely take $|Z'| \approx 1$. Solving Eq. (A7) shows that a value of $\xi \sim 7$–28 is the solution within the allowed range of parameter space ($10^{-4} \lesssim \alpha' \lesssim 10^{-1}$). In Sec. V B 2, Eqs. (91), we obtain the most conservative lower bound on the mass of F_2 when $\xi = \xi_{\rm max} \approx 28$.

When analyzing the process of K-shell dark photoionization, Eqs. (91), we obtain the most conservative upper bound on the mass of F_2 when ξ assumes its lowest possible value. In this case we find that, to a reasonable approximation, $\xi_{\rm min} \approx \min[1/(\alpha'^3 Z'^4), 1]$.

APPENDIX B: DARK THOMSON SCATTERING AND HALO HEATING

In the paper we assumed that the dark photons arising from kinetic mixing induced processes in the core of ordinary supernovae heat the halo via a dark photoionization process. In principle, one could consider dark Thomson scattering ($\gamma_D F_1 \rightarrow \gamma_D F_1$, where F_1 denotes a free F_1 particle) as an equally viable heating mechanism. However, we will show below that this is not expected to be the case for the parameter space of interest.

The optical depth for dark Thomson scattering, considering a dark photon propagating from the center of the galaxy to infinity, is given by

$$\tau = \int_0^\infty dr \sigma_{\rm DT} n_{F_1}$$

$$= \int_0^\infty dr \sigma_{\rm DT} \rho \kappa(|Z'| - 2)$$

$$= \frac{4\pi^2 \alpha'^2 \kappa(|Z'| - 2)\rho_0 r_0}{3m_{F_1}^2}, \qquad (B1)$$

where we have related the free F_1 number density to the density profile via the relation $n_{F_1} \approx \rho \kappa(|Z'| - 2)$ and made use of the expression for the dark Thomson scattering cross section $\sigma_T = 8\pi \alpha'^2/(3m_{F_1}^2)$.

Assuming the spectrum of dark photons that heat the halo has energy spectrum that peaks well below the electron mass, kinematic considerations dictate that dark Thomson scattering can only efficiently impart energy to the scattered F_1 particles provided that $\tau \gg 1$ (i.e. the dark photon becomes trapped within the galaxy), and hence if

$$m_{F_2} \ll \frac{4\pi^2 \rho_0 r_0}{3} \frac{\alpha'^2 |Z'|}{m_{F_1}^2}. \tag{B2}$$

Here we have used $\kappa \approx 1/m_{F_2}$ [from Eq. (70)]. Recall that the basic requirement that the halo be ionized gave a lower bound on m_{F_2} [Eqs. (91)]. Requiring that the above upper bound on m_{F_2} [Eq. (B2)] be greater than the lower bound found in Eqs. (91), we find

$$m_{F_1}^3 \ll \frac{4\pi^2 \rho_0 r_0 v_{\rm rot}^2 \xi_{\rm max}}{3}. \tag{B3}$$

Equation (B3) reduces to

$$\frac{m_{F_1}}{\rm MeV} \ll \left(\frac{\rho_0 r_0}{100\,\frac{\rm M_\odot}{\rm pc^2}}\right)^{\frac{1}{3}} \left(\frac{v_{\rm rot}}{300\ {\rm km/s}}\right)^{\frac{2}{3}}. \tag{B4}$$

This is the condition for dark Thomson scattering to be a viable heating mechanism. It follows that dark Thomson scattering is not expected to be an important heating mechanism for any spirals ($v_{\rm rot} \lesssim 300$ km/s) if $m_{F_1} \gtrsim 0.1$ MeV, which is the parameter range we are focusing on.

[1] V. C. Rubin and W. K. Ford, Jr., Astrophys. J. **159**, 379 (1970); V. C. Rubin, N. Thonnard, and W. K. Ford, Jr., Astrophys. J. **238**, 471 (1980).

[2] A. Refregier, Annu. Rev. Astron. Astrophys. **41**, 645 (2003); S. Cole et al. (2dFGRS Collaboration), Mon. Not. R. Astron. Soc. **362**, 505 (2005); W. J. Percival et al. (2dFGRS Collaboration), Mon. Not. R. Astron. Soc. **327**, 1297 (2001).

[3] S. Dodelson, Modern Cosmology (Academic Press, Amsterdam, 2003).

[4] J. L. Feng, H. Tu, and H.-B. Yu, J. Cosmol. Astropart. Phys. 10 (2008) 043; J. L. Feng, M. Kaplinghat, H. Tu, and H. B. Yu, J. Cosmol. Astropart. Phys. 07 (2009) 004.

[5] D. E. Kaplan, G. Z. Krnjaic, K. R. Rehermann, and C. M. Wells, J. Cosmol. Astropart. Phys. 05 (2010) 021; 10 (2011) 011; J. M. Cline, Z. Liu, and W. Xue, Phys. Rev. D **85**, 101302 (2012); F. Y. Cyr-Racine and K. Sigurdson, Phys. Rev. D **87**, 103515 (2013); J. M. Cline, Z. Liu, G. Moore, and W. Xue, Phys. Rev. D **90**, 015023 (2014).

[6] A. Ibarra, A. Ringwald, and C. Weniger, J. Cosmol. Astropart. Phys. 01 (2009) 003; S. Andreas, M. D. Goodsell, and A. Ringwald, Phys. Rev. D **87**, 025007 (2013); AIP Conf. Proc. **1563**, 114 (2013); N. Arkani-Hamed, D. P. Finkbeiner, T. R. Slatyer, and N. Weiner, Phys. Rev. D **79**, 015014 (2009).

[7] J. W. Cui, H. J. He, L. C. Lu, and F. R. Yin, Phys. Rev. D **85**, 096003 (2012).

[8] R. Foot, H. Lew, and R. R. Volkas, Phys. Lett. B **272**, 67 (1991).

[9] Z. Berezhiani, D. Comelli, and F. L. Villante, Phys. Lett. B **503**, 362 (2001); A. Yu. Ignatiev and R. R. Volkas, Phys. Rev. D **68**, 023518 (2003); Z. Berezhiani, P. Ciarcelluti, D. Comelli, and F. L. Villante, Int. J. Mod. Phys. D **14**, 107 (2005); P. Ciarcelluti, arXiv:astro-ph/0312607.

[10] R. Foot, Int. J. Mod. Phys. D **13**, 2161 (2004).

[11] R. Foot and R. R. Volkas, Phys. Rev. D **70**, 123508 (2004).

[12] R. Foot, Phys. Dark Univ. **5**, 236 (2014); Phys. Rev. D **88**, 023520 (2013); , J. Cosmol. Astropart. Phys. 12 (2014) 047.

[13] R. Bernabei et al., Riv. Nuovo Cimento **26N1**, 1 (2003); Eur. Phys. J. C **56**, 333 (2008); , Eur. Phys. J. C **73**, 2648 (2013).

[14] C. E. Aalseth et al., Phys. Rev. Lett. **107**, 141301 (2011); C. E. Aalseth et al. (CoGeNT Collaboration), arXiv:1401.3295.

[15] R. Foot, Phys. Rev. D **82**, 095001 (2010); Phys. Lett. B **728**, 45 (2014).

[16] R. Foot, Phys. Rev. D **90**, 121302 (2014).

[17] R. Foot, Int. J. Mod. Phys. A **29**, 1430013 (2014).

[18] K. Petraki and R. R. Volkas, Int. J. Mod. Phys. A **28**, 1330028 (2013); K. M. Zurek, Phys. Rep. **537**, 91 (2014).

[19] R. Foot and X. G. He, Phys. Lett. B **267**, 509 (1991).

[20] B. Holdom, Phys. Lett. **166B**, 196 (1986).

[21] R. Foot, Phys. Rev. D **88**, 025032 (2013).

[22] K. Petraki, L. Pearce, and A. Kusenko, J. Cosmol. Astropart. Phys. 07 (2014) 039.

[23] H. Goldberg and L. J. Hall, Phys. Lett. B **174**, 151 (1986).

[24] J. Fan, A. Katz, L. Randall, and M. Reece, Phys. Rev. Lett. **110**, 211302 (2013); J. Fan, A. Katz, and J. Shelton, J. Cosmol. Astropart. Phys. 06 (2014) 059.

[25] G. G. Raffelt, Stars as Laboratories for Fundamental Physics: The Astrophysics of Neutrinos, Axions, and Other Weakly Interacting Particles (University of Chicago Press, Chicago, 1996).

[26] S. Davidson, S. Hannestad, and G. Raffelt, J. High Energy Phys. 05 (2000) 003.

[27] R. Foot, A. Kobakhidze, K. L. McDonald, and R. R. Volkas, Phys. Rev. D **89**, 115018 (2014); see also R. R. Volkas, A. J. Davies, and G. C. Joshi, Phys. Lett. B **215**, 133 (1988).

[28] G. 't Hooft, in Proceedings of 1979 Carg'ese Institute on Recent Developments in Gauge Theories (Plenum Press, New York, 1980), p. 135.

[29] M. I. Dobroliubov and A. Y. Ignatiev, Phys. Rev. Lett. **65**, 679 (1990).

[30] J. Bernstein, M. Ruderman, and G. Feinberg, Phys. Rev. **132**, 1227 (1963); J. R. Ellis and K. A. Olive, Nucl. Phys. **B223**, 252 (1983).

[31] S. Davidson, B. Campbell, and D. C. Bailey, Phys. Rev. D **43**, 2314 (1991).

[32] E. W. Kolb, D. Seckel, and M. S. Turner, Nature (London) **314**, 415 (1985); H. M. Hodges, Phys. Rev. D **47**, 456 (1993); Z. G. Berezhiani, A. D. Dolgov, and R. N. Mohapatra, Phys. Lett. B **375**, 26 (1996).

[33] H. Vogel and J. Redondo, J. Cosmol. Astropart. Phys. 02 (2014) 029.

[34] R. Foot, Phys. Lett. B **711**, 238 (2012).

[35] E. D. Carlson and S. L. Glashow, Phys. Lett. B **193**, 168 (1987).

[36] P. Ciarcelluti and R. Foot, Phys. Lett. B **679**, 278 (2009).

[37] P. Gondolo and G. Gelmini, Nucl. Phys. **B360**, 145 (1991).

[38] E. W. Kolb and M. S. Turner, The Early Universe, Frontiers in Physics Vol. 69 (Westview Press, Boulder, 1990), p. 1.

[39] R. P. Feynman, R. B. Leighton, and M. Sands, Feynman Lectures on Physics (Addison-Wesley, Reading, MA, 1964), Vol. 1.

[40] G. Mangano, G. Miele, S. Pastor, T. Pinto, O. Pisanti, and P. D. Serpico, Nucl. Phys. **B729**, 221 (2005).

[41] E. Komatsu et al. (WMAP Collaboration), Astrophys. J. Suppl. Ser. **192**, 18 (2011).

[42] R. Keisler et al., Astrophys. J. **743**, 28 (2011).

[43] J. Dunkley et al., Astrophys. J. **739**, 52 (2011).

[44] P. A. R. Ade et al. (Planck Collaboration), Astron. Astrophys. **571**, A16 (2014).

[45] S. Weinberg, Cosmology (Oxford University Press, Oxford, UK, 2008).

[46] J. Bernstein, L. S. Brown, and G. Feinberg, Rev. Mod. Phys. **61**, 25 (1989).

[47] Y. I. Izotov and T. X. Thuan, Astrophys. J. **710**, L67 (2010); E. Aver, K. A. Olive, and E. D. Skillman, J. Cosmol. Astropart. Phys. 05 (2010) 003.

[48] K. Petraki, M. Trodden, and R. R. Volkas, J. Cosmol. Astropart. Phys. 02 (2012) 044.

[49] R. Foot, Phys. Lett. B **718**, 745 (2013).

[50] P. Ciarcelluti and Q. Wallemacq, Phys. Lett. B **729**, 62 (2014).

[51] J. Beringer et al. (Particle Data Group Collaboration), Phys. Rev. D **86**, 010001 (2012).

[52] R. Foot and Z. K. Silagadze, Int. J. Mod. Phys. D **14**, 143 (2005).

[53] M. Schmidt, Astrophys. J. **129**, 243 (1959).

[54] G. B. Rybicki and A. P. Lightman, Radiative Processes in Astrophysics (Wiley, New York, 2008).

[55] K. C. Freeman, Astrophys. J. **160**, 811 (1970).

[56] W. J. G. de Blok, Adv. Astron. **2010**, 789293 (2010).

[57] F. Donato and P. Salucci, Mon. Not. R. Astron. Soc. **353**, L17 (2004).

[58] W. Li, R. Chornock, J. Leaman, A. V. Filippenko, D. Poznanski, X. Wang, M. Ganeshalingam, and F. Mannucci, Mon. Not. R. Astron. Soc. **412**, 1473 (2011).

[59] M. J. Meyer, M. A. Zwaan, R. L. Webster, S. Schneider, and L. Staveley-Smith, Mon. Not. R. Astron. Soc. **391**, 1712 (2008).

[60] R. B. Tully and J. R. Fisher, Astron. Astrophys. **54**, 661 (1977).

[61] D. Maoz, Astrophysics in a Nutshell (Princeton University Press, Princeton, NJ, 2007).

[62] F. Shankar, A. Lapi, P. Salucci, G. De Zotti, and L. Danese, Astrophys. J. **643**, 14 (2006).

[63] P. Salucci, A. Lapi, C. Tonini, G. Gentile, I. Yegorova, and U. Klein, Mon. Not. R. Astron. Soc. **378**, 41 (2007).

[64] J. Kormendy and K. C. Freeman, in Scaling Laws for Dark Matter Halos in Late-Type and Dwarf Spheroidal Galaxies, International Astronomical Union Symposium, July, Sydney, Australia, 2003, edited by S. D. Ryder, D. J. Pisano, M. A. Walker, and K. C. Freeman [Astronomical Society of the Pacific, Vol. 220, p. 337 (2004)].

[65] F. Donato, G. Gentile, P. Salucci, C. Frigerio Martins, M. I. Wilkinson, G. Gilmore, E. K. Grebel, A. Koch, and R. Wyse, Mon. Not. R. Astron. Soc. **397**, 1169 (2009).

[66] S. M. Faber and R. E. Jackson, Astrophys. J. **204**, 668 (1976).

[67] R. A. Ibata et al., Nature (London) **493**, 62 (2013), and references therein.

[68] M. S. Pawlowski, J. Pflamm-Altenburg, and P. Kroupa, Mon. Not. R. Astron. Soc. **423**, 1109 (2012), and references therein.

[69] P. Kroupa, B. Famaey, K. S. de Boer, J. Dabringhausen, M. S. Pawlowski, C. M. Boily, H. Jerjen, D. Forbes, G. Hensler, and M. Metz, Astron. Astrophys. **523**, A32 (2010).

[70] R. Foot and Z. K. Silagadze, Phys. Dark Univ. **2**, 163 (2013).

[71] G. Gentile, P. Salucci, U. Klein, and G. L. Granato, Mon. Not. R. Astron. Soc. **375**, 199 (2007).

[72] R. Foot and S. Vagnozzi, arXiv:1412.0762.

[73] W. Lotz, Z. Phys. **216**, 241 (1968).

[74] Y. S. Kim and R. H. Pratt, Phys. Rev. A **27**, 2913 (1983).